Main Manuscript for

NEUROPILIN-1 IS A CO-RECEPTOR FOR NGF AND TRKA-EVOKED PAIN

Chloe J. Peach[1,2], Raquel Tonello[1,2], Kimberly Gomez[1,2], Aida Calderon-Rivera[1,2], Renato Bruni[1,2], Harsh Bansia[1,2], Laura Maile[3], Ana-Maria Manu[1,2], Hyunggu Hahn[1,2], Alex R.B. Thomsen[1,2], Brian L. Schmidt[1,2,4,5], Steve Davidson[3], Amedee des Georges[1,2], Rajesh Khanna[1,2,6], *Nigel W. Bunnett[1,2,6]

[1]Department of Molecular Pathobiology, College of Dentistry, New York University; [2]Pain Research Center, New York University; [3]Department of Anesthesiology, College of Medicine, University of Cincinnati, Cincinnati, USA, [4]Translational Research Center, College of Dentistry, New York University; [5]Department of Oral and Maxillofacial Surgery, College of Dentistry, New York University; [6]Department of Neuroscience and Physiology, Neuroscience Institute, Grossman School of Medicine, New York University

***Correspondence:** Nigel W. Bunnett, PhD. Room 724, 433 1st Avenue, New York, 10010, USA.

Email: nwb2@nyu.edu

Author Contributions: C.J.P., R.T., K.G., A.C-R, R.B., H.B., L.M. and A.M. conducted experiments and analyzed results; H.H., A.R.B.T. provided reagents; C.J.P., B.L.S., S.D., A.d.G., R.K. and N.W.B. designed experiments, wrote the manuscript and obtained funding.

Competing Interest Statement: Nigel W. Bunnett is a founding scientist of Endosome Therapeutics. Research in his laboratory is funded in part by Takeda Therapeutics.

Classification: Biological Sciences; Pharmacology.

Keywords: Pain, Signal Transduction, Neuroscience

This PDF file includes:

Main Text

Figures 1 to 9

Abstract

Nerve growth factor (NGF) monoclonal antibodies are a treatment for chronic pain yet failed to gain FDA approval due to worsened joint damage in some osteoarthritis patients. We report that neuropilin-1 (NRP1) is a nociceptor-enriched co-receptor for NGF that is necessary for tropomyosin-related kinase A (TrkA) signaling of pain. NGF binds NRP1 with nanomolar affinity. NRP1 is coexpressed with TrkA in human and mouse nociceptors. NRP1 inhibitors prevent NGF-stimulated excitation of human and mouse nociceptors and abrogate NGF-evoked nociception in mice. NRP1 knockdown blunts NGF-stimulated TrkA phosphorylation, kinase signaling and transcription, whereas NRP1 overexpression enhances NGF and TrkA signaling. As well as interacting with NGF, NRP1 associates with and chaperones TrkA from the biosynthetic pathway to the plasma membrane and then to signaling endosomes, which enhances NGF-induced TrkA dimerization, endocytosis and signaling. Molecular modeling supports interaction of a C-terminal basic NGF motif (R/KXXR/K) with an extracellular “b” NRP1 domain within an NGF/TrkA/NRP1 plasma membrane complex with a 2:2:2 stoichiometry. G Alpha Interacting Protein C-terminus 1 (GIPC1), a PDZ-binding protein that scaffolds NRP1 and TrkA to myosin VI, is coexpressed in nociceptors with NRP1 and TrkA. Knockdown of GIPC1 abrogates NGF-evoked excitation of nociceptors and pain-like behavior in mice. Thus, NRP1 is a previously unrecognized co-receptor necessary for NGF/TrkA pain signaling. NRP binds NGF and chaperones TrkA to the plasma membrane and signaling endosomes *via* the adaptor protein GIPC1. Antagonism of NRP1 and GIPC1 in nociceptors offers a long-awaited non-opioid alternative to systemic antibody NGF sequestration for the treatment of pain.

Significance Statement

Although monoclonal antibodies to nerve growth factor (NGF) reduce pain in patients with osteoarthritis, they failed to gain FDA approval due to the deleterious consequences of sequestrating NGF throughout the body. We report that neuropilin 1 (NRP1) is an alternative target for the treatment of NGF-dependent pain. NRP1 and the NGF receptor, tropomyosin-related kinase A (TrkA), are coexpressed in neurons that that detect painful stimuli in humans and mice. NRP1 binds NGF and escorts TrkA to the surface of pain-sensing nerves. NRP1 antagonism prevents NGF- and TrkA-mediated pain. The identification of NRP1 as an NGF receptor that is enriched in pain-sensing nerves reveals an alternate and much-needed target for the treatment of the multiple forms of NGF-evoked pain.

Main Text

Introduction

The first discovered growth factor, nerve growth factor (NGF), was identified by its ability to stimulate growth of sympathetic neurons (1). Tropomyosin-related kinase A (TrkA), a receptor tyrosine kinase (RTK), mediates these neurotrophic actions of NGF (2). After NGF binds to TrkA at peripheral nerve terminals, stable NGF/TrkA signalosomes are transported in a retrograde direction to the distant neuronal soma, where they regulate transcription and neuronal development (3, 4). NGF and TrkA are also strongly implicated in multiple forms of pain (5). $p75^{NTR}$ is another receptor for NGF as well as the immature pro-peptide (6, 7) that activates opposing pro-apoptotic signaling pathways (8). Although NGF and its receptors have been intensively studied in the context of neuronal development and pain, mechanistic gaps in understanding have hampered the successful approval of NGF-directed therapeutics.

Chronic pain afflicts twenty percent of the global population at some point in life, yet is inadequately treated by opioids and non-steroidal anti-inflammatory drugs, which lack efficacy and have life-threatening side effects. NGF/TrkA is one of the few non-opioid targets for chronic pain

validated in patients. NGF, which is produced by injured and diseased tissues, activates TrkA on peripheral nociceptors to evoke rapid sensitization and stimulate the transcription of neuropeptides, receptors and ion channels that mediate pain (5). NGF-stimulated neuronal sprouting may also contribute to pain and accompanies painful conditions (5). NGF and TrkA have been implicated in pain associated with inflammation, nerve injury and cancer (5). The central role of TrkA and NGF in pain is evident in patients with Hereditary Sensory and Autonomic Neuropathy (HSAN) Type IV and V, where pathological insensitivity to pain results from loss-of-function mutations in TrkA (9) and NGF (10), respectively. Although monoclonal antibodies (mAbs) are analgesic in osteoarthritic patients (11), they lack FDA approval due to worsening joint damage in some individuals (12). The identification of nociceptor-enriched mediators of NGF-induced pain may facilitate development of non-opioid analgesics, avoiding the adverse effects of systemic NGF sequestration with mAbs.

Transcriptome analyses have identified proteins that are conserved between rodent and human nociceptors, including neuropilin-1 (NRP1) (13). NRP1 is a type I transmembrane protein discovered for its role in axon guidance (14). Lacking a catalytic domain, NRP1 does not transduce signals *per se* but rather acts as a co-receptor for unrelated families of proteins, including vascular endothelial growth factor (VEGF-A) (15). NRP1 is a co-receptor with VEGF receptor 2 (VEGFR2) that enhances VEGF-A-induced blood vessel development. NRP1 overexpression in cancers spurred the development of a mAb, vesencumab/MNRP1685A, to inhibit tumorigenesis (16). NRP1 is also implicated in VEGF-A-mediated pain (17, 18). Since NGF, a major pain mediator, possesses a prospective NRP1 binding motif, we investigated the hypothesis that NRP1 is a co-receptor for NGF and TrkA in nociception.

Results

NRP1 binds human β-NGF

NRP1 is a co-receptor for unrelated families of proteins including neuronal guidance molecules (semaphorins) (19), growth factors (VEGF-A) (15), cell-penetrating peptides (20), and viruses (SARS-CoV-2) (14). NRP1 ligands share a C-terminal basic motif (C-end rule, “CendR” motif, R/KXXR/K), which interacts with extracellular “b” domains of NRP1 (15, 19). Inspection of the amino acid sequence of mature NGF identified prospective ‘CendR’ R/KxxR/K motifs within the C-terminus that are conserved between rodents and humans and known to mediate the interaction of other growth factors with NRP1 (20) (**Fig. 1A**).

To directly investigate whether NGF binds NRP1, microscale thermophoresis (MST) was used to analyze interactions between fluorescent human NGF and the extracellular a1a2b1b2 domain of human NRP1. NGF interacted with NRP1 with low nanomolar affinity (K_d = 35.5 ± 4.7 nM, n=4, **Fig. 1B**). No interaction was detected between fluorescent NGF and staphylokinase (negative control). The measured NGF/NRP1 affinity is lower than the reported affinities of NGF for TrkA and $p75^{NTR}$, which are in the in the 1-15 nM range using surface plasmon resonance (21, 22), but is comparable to affinity of $VEGF_{165}a$ for NRP1 (K_d 9 nM (23) to 120 nM (24)).

NGF binding to NRP1 in living cells at 37ºC was analyzed using a modified bioluminescence resonance energy transfer (BRET)-based assay (**Fig. 1C**). $VEGF_{165}a$ (positive control growth factor known to interact with NRP1) or NGF was genetically fused to an 11 amino acid fragment (HiBiT) of nanoluciferase (NanoLuc). HiBiT has a high affinity for the complementary LgBiT fragment. HiBiT-tagged growth factors were expressed in HEK293T cells, secreted into supernatant, and conjugated to recombinant LgBiT to form full length and catalytically active NanoLuc. Upon addition of furimazine substrate, complemented NanoLuc emits bioluminescence. This supernatant containing HiBiT-tagged growth factor was incubated with cells expressing SnapTag-NRP1 labeled with SNAP-Surface® Alexa Fluor® 488 fluorophore (SnapTag-AF488, +) or lacking fluorophore (-). If proteins are in close proximity (<10 nm), luminescent growth factor can act as a BRET donor to fluorescent NRP1. As a positive control, BRET was detected between luminescent $VEGF_{165}a$ and SnapTag-NRP1 (**Fig. 1D**). Pre-incubation of cells with an excess of

$VEGF_{165}a$ (10 nM) abolished the BRET signal. No BRET signal was detected when luminescent $VEGF_{165}a$ was incubated with cells expressing a binding-dead NRP1 mutant in the b1 domain (25, 26). Importantly, BRET was detected between NGF-HiBiT and SnapTag-NRP1, and pre-incubation with unlabeled $VEGF_{165}a$ inhibited this response.

The results from analysis of interactions between recombinant proteins and ligand binding studies in intact cells provide evidence that NGF directly binds NRP1 with nanomolar affinity.

Modeling an NGF/TrkA/NRP1 ternary complex

Ternary complexes of human NGF/TrkA/NRP1 were generated through an information-driven computational docking protocol using HADDOCK 2.4 (27). The complexes were analyzed against available biochemical data. Binding interactions of sterically feasible complexes in the cellular context were then analyzed at the molecular level. NRP1 is composed of five extracellular domains from N- to C-terminus, namely a1, a2, b1, b2 and c/MAM (28). The extracellular domain (ECD) of TrkA comprises an N-terminal leucine-rich repeat (LRR) domain and C-terminal immunoglobulin domains (Ig-C1, Ig-C2) (29). The crystal structure of NGF/TrkA complex reveals a 2:2 stoichiometry (PDB 2IFG). Our docked model of NGF/TrkA/NRP1 suggests a 2:2:2 stoichiometry with one NRP1 molecule interacting with one TrkA molecule and the NGF dimer (**Fig. 1E, Table S1**). The model suggests that the NRP1 b1 domain predominantly interacts with the NGF C-terminus while also interfacing with an interdomain region between Ig-C1 and Ig-C2 domains of TrkA. In this model, the NRP1 a1 and a2 domains interface with the top of the TrkA LRR domain and the NRP1 b2 domain slots in the curved space between TrkA Ig-C1 and LRR domains contributing to shape complementarity between TrkA and NRP1 (**Fig. 1E**). hNGF has two prospective 'CendR' R/KxxR/K motifs within the C-terminus that mediate interaction of other growth factors with NRP1 b1 domains (20, 30, 31). We observed that in this model R118 from CendR motif $K_{115}AVR_{118}$ binds to C-terminal arginine binding pocket located in the NRP1 b1 domain through molecular interactions, including hydrogen bonding interactions between NGF R118 and NRP1 conserved residues Y297, D320 and Y353 (**Fig. 1E inset**). NRP-binding proteins and peptides possess a C-terminal arginine that binds to a specific C-terminal arginine binding pocket of the NRP1 b1 domain through similar set of molecular interactions (31, 32). The membrane proximal MAM domain of NRP1, extending from the NRP1 b2 domains, is proposed to orient the other extracellular domains of NRP1 away from the membrane for protein/protein interaction (28). In the NGF/TrkA/NRP1 docked model, the NRP1 b2 domain lies perpendicular to the NGF/TrkA 2-fold symmetry axis with solvent accessible C-termini pointing towards the membrane (**Fig. 1E**). This orientation suggests that it is possible to extend the MAM domain from the b2 domain towards the membrane while NRP1 is still bound to the NGF/TrkA complex resulting in a sterically permissible membrane tethered NGF/TrkA/NRP1 complex (**Fig. 1F**). TrkA Asn-linked glycosylation can regulate its localization and activity (33). Although non-standard residues were excluded from docking calculations, the NGF/TrkA/NRP1 docked model shows that NRP1 binding to TrkA does not clash with Asn-linked glycosylations on TrkA suggesting sterically feasible binding of NRP1 to glycosylated TrkA in a cellular context (**Fig. S1**). Thus, our analysis provides structural insights into the NRP1 co-receptor function for NGF/TrkA signaling analogous to a recent structural study of NRP1 co-receptor function with an unrelated family of proteins (34).

***Ntrk1*/TrkA and *Nrp1*/NRP1 are co-expressed in mouse and human DRG neurons**

To determine whether NRP1 could function as an NGF/TrkA co-receptor in nociceptors, TrkA and NRP1 were localized in mouse and human dorsal root ganglia (DRG) by immunofluorescence (protein) and RNAScope™ *in situ* hybridization (mRNA). In mice, immunoreactive TrkA was detected in vesicles and immunoreactive NRP1 was localized at the plasma membrane of the same DRG neurons (**Fig. 2A**). *Ntrk1* (TrkA) and *Nrp1* (NRP1) mRNAs also colocalized in mouse DRG neurons, which were identified by NeuN immunostaining (**Fig. 2B**). *Nrp1* was detected in 42% of small-diameter peptidergic nociceptors of mouse DRG that expressed immunoreactive calcitonin-gene-related peptide (CGRP) (**Fig. 2C**). In humans, *Ntrk1* and *Nrp1* mRNAs also colocalized in DRG neurons (**Fig. 2D**). *Nrp1* was detected in 59% of human DRG that

expressed immunoreactive CGRP and 42% of neurons expressing P2X purinoceptor 3 (P2X3) (**Fig. 2E**). In mice, *Nrp1* mRNA was expressed in 33% of *Ntrk1*-positive neurons (**Fig. 2F**). In humans, *Nrp1* was co-expressed in 93% of *Ntrk1*-positive neurons (**Fig. 2G**). Thus, TrkA and NRP1 are co-expressed in the same neurons in DRG in mouse and human, where NRP1 is appropriately located to control NGF/TrkA signaling.

NRP1 antagonism abrogates NGF-induced ionic currents in mouse and human DRG neurons

NGF/TrkA signaling promotes pain by kinase-mediated phosphorylation and sensitization of ion channels, leading to enhanced sensitivity to mechanical, thermal and chemical stimuli, thus activating voltage-gated ion channels in DRG neurons (5). Patch-clamp recordings under current-clamp mode were made to determine whether NRP1 is necessary for NGF-induced excitability and ion channel activity in dissociated DRG neurons. Exposure of mouse DRG neurons to murine NGF (50 nM), stimulated action potential firing of nociceptors elicited by a depolarizing ramp pulse (**Fig. 3A, B**). Pre-incubation with the NRP1 inhibitor EG00229 (30 µM) (25) prevented NGF-induced hyperexcitability (**Fig. 3A, B**). NGF or EG00229 did not affect the resting membrane potential (**Fig. 3C**) or the rheobase, the minimum current necessary to elicit an action potential (**Fig. 3D**).

Since both Ca^{2+} and Na^{+} channels have critical roles in controlling the excitability of sensory neurons, we further tested whether NGF increased the activity of voltage-gated ion channels by making patch-clamp recordings under the voltage-clamp mode in dissociated mouse DRG. NGF (50 nM) increased total Ca^{2+} currents (**Fig. 3E**) and current density (**Fig. 3F, G**) by ~50% when compared to vehicle (DMSO)-treated cells. EG00229 prevented NGF-induced activation of Ca^{2+} currents, but had no effect on Ca^{2+} currents in unstimulated DRGs (**Fig. 3F, G**). Half-maximal activation and inactivation ($V_{1/2}$) potential, as well as slope factor values (k) for activation and inactivation, were not different between the conditions tested, except for an ~8-mV hyperpolarizing shift in Ca^{2+} channel activation induced by EG00229 when compared to DMSO- and NGF-treated DRGs (**Fig. 3H, Table S2**). Similarly, EG00229 normalized NGF-induced increases in Na^{+} currents (**Fig. 3I**). NGF caused a two-fold increase in Na^{+} current density (**Fig. 3J**) and peak current density (**Fig. 3K**) when compared to vehicle (DMSO)-treated DRG neurons. EG00229 abolished these effects of NGF but had no effects on Na^{+} currents in unstimulated DRGs (**Fig. 3J,K**). There were no detectable changes in the voltage-dependence of activation and inactivation between the conditions tested, except for a ~10-mV depolarizing shift in the $V_{1/2}$ of inactivation of EG00229 and NGF-treated cells compared to control (**Fig. 3L**). These data implicate voltage-gated Ca^{2+} and Na^{+} channels as downstream effectors of NRP1-mediated NGF signaling.

To assess human translation, the contribution of NRP1 to NGF-stimulated activation of dispersed human DRG neurons was similarly studied. Human NGF (50 nM) increased the number of action potentials elicited by a depolarizing ramp pulse (**Fig. 3M, N**). Pre-incubation with the NRP1 inhibitor EG00229 (30 µM) (25) prevented NGF-induced hyperexcitability (**Fig. 3M, N**). NGF or EG00229 did not affect the resting membrane potential (**Fig. 3O**) or the rheobase (**Fig. 3P**).

Thus, NRP1 is necessary for NGF-induced sensitization of nociceptors in rodents to humans.

NRP1 antagonism inhibits NGF-induced nociception in mice

NGF injection is known to induce pain in humans and rodents (5). In addition to sensitizing ion channels, NGF/TrkA signaling also promotes chronic pain through the upregulation of genes encoding neuropeptides, ion channels and receptors that mediate pain (*e.g.*, substance P, transient receptor potential vanilloid 1) (5). To test whether NRP1 is necessary for NGF-induced nociception, murine NGF (50 ng) was administered to mice by intraplantar (i.pl., 10 µl) injection (**Fig. 4A**). A human mAb against the b1b2 domain of NRP1 (vesencumab (16), 7 µg/10 µl) or control IgG (7 µg/10 µl), or small molecule NRP1 inhibitor EG00229 (30 µM/10 µl) (25) or compound 5 (Cpd-5; 30 µM/10 µl) (35) or vehicle (PBS, 10 µl) was co-administered (i.pl.) with NGF. Withdrawal responses of NGF-injected (ipsilateral) hindpaws to stimulation with von Frey filaments (VFF) and

radiant heat were assessed to evaluate mechanical allodynia and thermal hyperalgesia, respectively. In control experiments, NGF decreased the withdrawal threshold to VFF stimulation and the latency of withdrawal to thermal stimulation within 30 min for at least 4 h, indicating mechanical allodynia and thermal hyperalgesia (**Fig. 4B-G**). Vesencumab and EG00229 strongly inhibited NGF-induced mechanical allodynia for 2 h and Cpd-5 inhibited mechanical allodynia for 1 h (**Fig. 4B-C**). Vesencumab, EG00229 and Cpd-5 also inhibited NGF-induced thermal hyperalgesia for 1-2 h (**Fig. 4E-G).** None of the inhibitors affected the withdrawal responses of the ipsilateral paw to mechanical or thermal stimuli in mice that did not receive NGF (**Fig. 4B-G**).

NGF mediates inflammatory pain (5), providing an opportunity to determine whether NRP1 is necessary for the pronociceptive actions of endogenous NGF. Complete Freund's Adjuvant (CFA, 1 mg/ml, 10 µl, i.pl.) was injected into the hindpaw. Vesencumab mAb (7 µg/10 µl) or IgG Ctrl (7 µg/10 µl), or EG00229 (30 µM/10 µl) or PBS (10 µl) (i.pl.) was injected into the inflamed paw 48 h after CFA (**Fig. 4H**). CFA induced sustained mechanical allodynia and thermal hyperalgesia (**Fig. 4I-L**). Vesencumab, but not EG00229, reduced thermal hyperalgesia 1 h after treatment (**Fig. 4K,L**). Vesencumab inhibited mechanical allodynia compared to IgG control, with a maximal effect at 1 h, lasting up to 2 h post-injection (**Fig. 4I**). EG00229 also partially reversed mechanical allodynia compared with vehicle, with a maximum inhibitory effect at 1 h, lasting for up to 4 h (**Fig. 4J**). Thus, NRP1 is necessary for the pronociceptive actions of exogenous and endogenous NGF in mice.

NRP1 controls NGF and TrkA kinase signaling

NGF primarily signals through TrkA (29), a 'crab claw'-like RTK where NGF binds to extracellular immunoglobulin-like domains to induce conformational changes throughout the RTK dimer that initiate auto- and trans-phosphorylation of intracellular tyrosine residues (*e.g.,* Y490, Y785). To determine whether NRP1 controls NGF-stimulated phosphorylation of TrkA, a proximal and necessary component of TrkA signaling, dissociated mouse DRG neurons were stained with a phospho-specific antibody to TrkA phosphorylation at residue Y785 (equivalent to Y794 in mouse TrkA). NGF (100 nM, 15 min) stimulated a ~1.4-fold increase in the intensity TrkA phospho-Y785 immunofluorescence compared to vehicle (**Fig. 5A, B**). Pre-incubation with EG00229 (30 µM, 30 min) prevented NGF-stimulated phosphorylation of TrkA but had no effect on the basal unstimulated phosphorylation. These results support the hypothesis that NRP1 is necessary for NGF-induced activation of TrkA.

Activated TrkA stimulates extracellular signal-regulated kinase (ERK) phosphorylation, as well as AKT and phospholipase Cγ. In addition to triggering neuronal development, TrkA-induced ERK signaling contributes to NGF-induced sensitization of nociceptors and pain (5). The contribution of NRP1 to ERK activation was monitored in CAD.a cells, a neuron-like cell line modified from the Cath.a catecholaminergic cell line obtained from a murine tumor (36). While CAD.a cells lack TrkA expression, they contain $p75^{NTR}$ and NRP1 (**Fig. S2**). To probe NGF/TrkA ERK signaling with high spatial and temporal resolution, Förster resonance energy transfer (FRET) EKAR biosensors targeted to the cytosol or nucleus were coexpressed with human TrkA in CAD.a cells. EKAR biosensors contain a reversible substrate sequence separated by two fluorophores (**Fig. 5C**). NGF activated ERK in the cytosol and nucleus within 5 min for at least 20 min (**Fig. 5D**). NGF-induced ERK activation was concentration-dependent, with a higher potency for nuclear than cytosolic ERK (**Fig. 5E, F, Table S3**). Pre-incubation with EG00229 (30 µM) did not affect NGF activation of cytosolic ERK (**Fig. 5E**), but significantly reduced the potency for NGF activation of nuclear ERK (**Fig. 5F, Table S3**; NGF EC_{50}: DMSO control, ~8 pM; EG00229 ~98 pM; paired t-test, P=0.023).

The contribution of NRP1 to NGF-induced ERK signaling was also investigated by NRP1 overexpression with TrkA in HEK293T cells, which express low levels of these proteins. As in CAD.a cells, NGF activated ERK in the cytosol and nucleus of HEK293T cells (**Fig. 5G**). While NRP1 co-expression did not influence cytosolic ERK signaling (**Fig. 5H**), NRP1 expression significantly enhanced activation of nuclear ERK in response to low (1 pM) NGF concentrations

(**Fig. 4I**). The outcomes of nuclear ERK signaling were studied by expression of a transcriptional luciferase reporter, where a luminescent protein is produced downstream of an ERK promoter (**Fig. 4C**). NGF stimulated concentration-dependent ERK transcriptional activity with significantly higher potency in cells overexpressing TrkA and NRP1 compared to cells expressing TrkA alone (**Fig. 5J, Table S3**; NGF EC_{50}: TrkA alone, 214 pM; TrkA + NRP1, 71 pM; paired t-test, P=0.0004). NGF did not stimulate ERK transcriptional activity in cells expressing NRP1 alone, confirming lack of inherent signaling capability of NRP1 (**Fig. 5J**). These results support the notion that NRP1 enhances NGF-induced TrkA activation and signaling by pathways that underpin nociception. We next sought to determine the mechanism of NRP1-mediated potentiation of NGF/TrkA signaling.

NRP1 is a chaperone that forms a complex with TrkA to control trafficking from the biosynthetic pathway to the plasma membrane

In addition to directly binding NGF, NRP1 could amplify NGF/TrkA signaling by receptor/co-receptor interactions with TrkA, akin to its co-receptor function with VEGFR2 (37). Cell surface expression of human TrkA and NRP1 was measured by specific substrate-based labeling of enzymatic tags genetically fused to the extracellular N-terminus of either receptor. SnapTag-TrkA and HaloTag-NRP1 were expressed in HEK293T and CAD.a cells and covalently labeled with membrane-impermeant AlexaFluor® substrates, thereby selectively labeling receptors transported to the cell surface. SnapTag-TrkA and HaloTag-NRP1 were highly co-localized at the cell surface of HEK293T and CAD.a cells, with the latter also showing a high level of co-localization in subcellular compartments (**Fig. 6A**). Labeling specificity was confirmed in cells expressing TrkA or NRP1 alone (**Fig. S3**).

To investigate the formation of a heteromeric complex between TrkA and NRP1, BRET was measured in HEK293T cells expressing NanoLuc-NRP1 and SnapTag-TrkA. Extracellular N-terminal NanoLuc acts as an energy donor to excite a nearby SnapTag. Measurement of BRET between NanoLuc-NRP1 and increasing levels of SnapTag-TrkA revealed a hyperbolic relationship, indicative of assembly of a heteromeric complex between NanoLuc-NRP1 and SnapTag-TrkA (**Fig. 6B, C**). As a positive control, a hyperbolic BRET signal relationship was also detected between NanoLuc-$p75^{NTR}$, which is known to interact with TrkA (5), and increasing levels of SnapTag-TrkA. In contrast, there was a linear BRET signal between NanoLuc-NRP1 and increasing levels of SnapTag-calcitonin-like receptor (CALCRL), an unrelated transmembrane receptor for CGRP. To verify whether this relationship was observed with protein expression, data from a representative experiment quantifying cell surface SnapTag labeling also demonstrated a hyperbolic curve between TrkA and NRP1 (**Fig. 6C**). These results suggest that NRP1 and TrkA co-localize at the plasma membrane as a heteromeric complex.

Recruiting TrkA to the plasma membrane would enable increased access to extracellular growth factor. The effect of NRP1 on the cell surface expression of TrkA was determined using the membrane-impermeant SnapTag fluorophore to selectively label cell surface TrkA (**Fig. 6D**). NRP1 co-expression increased level of TrkA at the surface in HEK293T cells by 150 $\pm$ 43% and of CAD.a cells by 109 $\pm$ 4% (**Fig. 6E-G**). Enhanced bystander BRET, which capitalizes on the endogenous affinity of pairs of *Renilla*-tagged proteins to boost sensitivity (38), was used to quantify the effects of NRP1 expression on the localization of TrkA in different subcellular compartments of living cells. TrkA tagged on the C-terminus with Renilla luciferase (Rluc, BRET) was coexpressed in HEK293T or CAD.a cells with proteins resident of the plasma membrane (CAAX), early endosomes (Rab5a), recycling endosomes (Rab4a) and the cis-Golgi apparatus (Giantin) tagged with *Renilla* green fluorescent protein (RGFP) (**Fig. 6H**). In HEK293T cells, NRP1 expression significantly increased BRET between TrkA-Rluc8 and RGFP-CAAX and significantly decreased BRET between TrkA-Rluc8 and tdRGFP-Rab5a, tdRGFP-Rab4a and tdRGFP-Giantin (**Fig. 6I**). In CAD.a cells, NRP1 expression did not affect BRET between TrkA-Rluc8 and RGFP-CAAX but significantly decreased BRET between TrkA-Rluc8 and tdRGFP-Rab5a, tdRGFP-Rab4a and tdRGFP-Giantin (**Fig. 6J**). These results indicate that NRP1 expression causes a redistribution of TrkA from subcellular regions involved in receptor recycling or *de novo* export to the plasma membrane, consistent with a chaperone function. Control studies confirmed NRP1 was successfully expressed using a

HaloTag label, where NRP1 co-expression had no significant effect on overall TrkA expression (**Fig. S4A-D**). These results suggest that NRP1 acts as a chaperone for TrkA.

NRP1 enhances NGF-induced TrkA trafficking and dimerization

Upon NGF stimulation, TrkA traffics to endosomes by clathrin-dependent and -independent mechanisms. NGF/TrkA signalosomes are retrogradely transported in endosomes or multivesicular bodies to the soma of sympathetic neurons, where they mediate the neurotrophic actions of NGF (3, 4). To determine the effects of NRP1 on NGF-evoked endocytosis of TrkA, BRET was measured between TrkA-Rluc8 and plasma membrane marker RGFP-CAAX (**Fig. 7A**). NGF caused a concentration-dependent decrease in TrkA-Rluc8 and RGFP-CAAX BRET (EC_{50} ~870 pM), with 10-100 nM NGF inducing maximal decrease within 5 min that was sustained for 20 min, consistent with TrkA endocytosis (**Fig. 7B, Table S3**). Hypertonic (0.45 M) sucrose or the clathrin inhibitor pitstop 2 (30 µM) prevented NGF-induced endocytosis of TrkA (**Fig. 7C, D**). Co-expression of NRP1 with TrkA enhanced NGF-stimulated endocytosis of TrkA (**Fig. 7E, F**). This effect of NRP1 was observed at higher NGF concentrations (>10 nM), with minimal effect on the potency of NGF-induced endocytosis of TrkA (**Table S3**). NGF also stimulated concentration-dependent removal of TrkA from the plasma membrane of CAD.a cells (EC_{50} ~490 nM; pEC_{50} = 9.31 ± 0.18, n=4) that was inhibited by hypertonic sucrose and pitstop 2 (**Fig. 7G-J**). Knockdown of endogenous NRP1 with siRNA significantly inhibited NGF-induced endocytosis of TrkA in CAD.a cells (**Fig. 7K, L**). NRP1 knockdown was confirmed at a protein level using immunofluorescence in CAD.a cells, while there was no effect on TrkA expression (**Fig. S4E-F**). Thus, whereas NRP1 overexpression enhances agonist-stimulated endocytosis of TrkA in HEK293T cells, NRP1 knockdown has the opposite effect in CAD.a cells. The results are consistent with a chaperone role for NRP1 in NGF-stimulated endocytosis of TrkA.

Dimerization of TrkA is pivotal for NGF/TrkA signaling (5). The contribution of NRP1 to TrkA oligomerization was evaluated by measuring BRET between NanoLuc-TrkA and SnapTag-TrkA in HEK293T cells (**Fig. 7M**). Expression of increasing amounts of SnapTag-TrkA in HEK293T cells expressing a fixed amount of NanoLuc-TrkA produced a hyperbolic BRET signal, indicating oligomerization (**Fig. 7N**). NGF (30 nM) significantly enhanced this signal, consistent with agonist-evoked TrkA oligomerization. In cells expressing a fixed ratio of SnapTag-TrkA and NanoLuc-TrkA, NGF stimulated a concentration-dependent increase in BRET that was maximal after 5 min and sustained for at least 20 min (EC_{50} 15 nM; **Fig. 7O, Table S3**). While NGF had a lower potency with respect to dimerization than endocytosis, the kinetics of TrkA dimerization and endocytosis were similar. NRP1 overexpression enhanced TrkA oligomerization in response to higher NGF concentrations (>30 nM) (**Fig. 7P, Q**). As dimerization is the first step in RTK activation, with well-established evidence for TrkA signaling from endosomes, these results provide a mechanistic insight into the role of NRP1 in controlling TrkA signaling and trafficking.

GIPC1 mediates NRP1/TrkA interactions and NGF-induced pain signaling

While NRP1 lacks intrinsic catalytic activity, the short cytoplasmic C-terminus interacts with G Alpha Interacting Protein C-terminus 1 (GIPC1), or synectin, through a PDZ domain (39). GIPC1 also interacts with the membrane-proximal regions of TrkA (40). Thus, interaction with GIPC1 could underpin the co-receptor function of NRP1 in NGF/TrkA-evoked nociception. Analysis by RNAScope™ *in situ* hybridization revealed that *Gipc1* mRNA was expressed by all mouse DRG neurons (**Fig. 8A**). In humans, *Gipc1* was expressed by 100% of *Ntrk1*-positive neurons and *Ntrk1* was expressed by 85% of *Gipc1*-positive neurons (**Fig. 8B,C**).

GIPC1 is an intracellular adaptor protein that associates with receptors and channels to regulate their trafficking by interacting with the inwardly-directed myosin VI motor (41). To determine whether GIPC1 is necessary for the TrkA chaperone function of NRP1, BRET between TrkA-Rluc8 and RGFP-CAAX was measured in HEK293T cells after GIPC1 knockdown. GIPC1 siRNA inhibited NRP1-induced plasma membrane expression of TrkA (**Fig. 8D**). In CAD.a cells, preincubation with a GIPC1 inhibitor (300 µM CR1023 (42)) or a myosin VI inhibitor (50 µM TIP

(43)) reduced NGF-induced TrkA trafficking to the plasma membrane (**Fig. 8E, F**). Similarly, GIPC1 siRNA inhibited the maximal response of NGF-induced ERK signaling quantified using the downstream transcriptional reporter in CAD.a cells, with no effect on potency (**Fig. 8G**) (Ctrl siRNA pEC_{50} = 9.58 ± 0.03, GIPC1 siRNA pEC_{50} = 9.63 ± 0.09, n=5). GIPC1 siRNA also prevented NGF-induced action potential firing in mouse DRG nociceptors, determined by patch-clamp recordings (**Fig. 8H, I**). GIPC1 siRNA knockdown was confirmed at the mRNA level in HEK293T cells, CAD.a cells and DRG (**Fig. S5A-C**).

To evaluate the role of GIPC1 in NGF-induced nociceptive behavior, GIPC1 or control siRNA was administered to mice by intrathecal (i.t.) injection 48 h before NGF intraplantar injection (**Fig. 8J**). In mice treated with control siRNA, NGF (50 ng/10 µl, i.pl.) caused mechanical allodynia and thermal hyperalgesia in the ipsilateral paw within 30 min for at least 24 h (**Fig. 8K, L**). GIPC1 siRNA prevented NGF-evoked mechanical allodynia and thermal hyperalgesia (**Fig 8K, L**). NGF or siRNA administration did not affect withdrawal responses of the contralateral paw to mechanical stimuli (**Fig. 8M**). The nociceptive role of GIPC1 was also investigated in a preclinical model of inflammatory pain in mice. Control or GIPC1 siRNA was administered (i.t.) 24 h after CFA (i.pl.) (**Fig. 8N**). Knockdown of GIPC1 in DRG was confirmed using RNAScope™ *in situ* hybridization (**Fig. S5D**). GIPC1 siRNA inhibited CFA-induced mechanical allodynia and thermal hyperalgesia after 24 and 48 h (**Fig. 8O, P**). CFA or siRNA administration did not affect withdrawal responses of the contralateral paw to mechanical stimuli (**Fig. 8Q**). These results reveal a major role for GIPC1 in NGF-evoked pain.

Discussion

We report that NRP1 is a previously unrecognized co-receptor for NGF and TrkA that is necessary for NGF-induced nociception, demonstrated in both rodent and human tissue. NRP1 enhances NGF/TrkA signaling, since NRP1 inhibition abrogates the actions of NGF in intact mice, isolated nociceptors and cell lines, whereas NRP1 overexpression enhances TrkA signaling and trafficking. The results are consistent with evidence that NRP1 is a co-receptor for VEGF-mediated angiogenesis using pharmacological (24) or genetic (44) interventions. NRP1 is proposed to promote NGF/TrkA-mediated pain by at least two mechanisms: as a coreceptor that directly binds NGF, and as a chaperone that assembles a heterodimeric complex to enhance TrkA trafficking to and from the plasma membrane (**Fig. 9**).

The coreceptor function of NRP1 is supported by nanomolar affinity binding measurements between recombinant NRP1 and NGF. Molecular modeling indicates that the “CendR” motif of NGF remains exposed when interacting with TrkA (29), which could allow assembly of a trimeric NGF/TrkA/NRP1 complex with a 2:2:2 stoichiometry. Structural analysis of the putative NGF/TrkA/NRP1 complex will be required to confirm this predicted model. Despite the glycosylated nature of NRP1, indirect association of NGF with matrix components is unlikely to mediate NGF/NRP1 interactions as NGF does not directly interact with the extracellular matrix (45). NRP1 potentiation of VEGFR2 signaling is linked to growth factor binding kinetics (26), similar to $p75^{NTR}$ potentiation of NGF/TrkA binding kinetics (46). Further studies of the effects of NRP1 on NGF/TrkA binding kinetics are warranted. Since the NGF/$p75^{NTR}$ binding site (47) does not directly conflict with the proposed NGF/NRP1 binding site, a TrkA/$p75^{NTR}$/NRP1 complex could interact with NGF, although there could be steric clashes between NRP1 and $p75^{NTR}$ for the same binding site on NGF.

The chaperone function of NRP1 is supported by BRET proximity assays showing that NRP1 and TrkA form a heteromeric complex and that NRP1 re-routes TrkA from the biosynthetic pathway to the plasma membrane and subsequently signaling endosomes. NRP1 colocalizes with TrkA to a greater extent than with VEGFR2 (37). Further studies are required to identify potential NRP1/TrkA interaction sites. TrkA redistribution to the cell surface would amplify exposure to extracellular NGF. Accordingly, NRP1 potentiates the effects of NGF on TrkA dimerization and endocytosis.

GIPC1 is a previously unrecognized mediator of pain. In the context of NGF/TrkA-evoked pain, GIPC1 interacts with TrkA (40) and NRP1 (39), and could thus scaffold TrkA/NRP1 interactions to facilitate NGF signaling. GIPC1 disruption abrogates NRP1-stimulated translocation of TrkA to the plasma membrane and inhibits NGF-evoked endocytosis of TrkA and ERK signaling, in line with reports in other systems (48). Considering GIPC1 regulates the trafficking of many receptors and ion channels, other mechanisms could mediate the antinociceptive effects of GIPC1 knockdown. Crucially, NRP1 and GIPC1 prominently colocalize with TrkA in human nociceptors where they could mediate NGF-induced pain. NRP1 may also serve as a co-receptor for NGF/TrkA signaling from adjacent cells, akin to VEGFR2 modulation from both 'cis' (same cell) and 'trans' (neighboring cell) forms (49). This intercellular signaling may underlie functional interactions between nociceptors and adjacent cells that contribute to pain (*e.g.,* Schwann cells).

Electrophysiological and behavioral studies support the essential role of NRP1 and GIPC1 in NGF-induced pain. Two chemically distinct small molecule NRP1 inhibitors and a mAb against the b1 domain of NRP1 prevent NGF-evoked mechanical allodynia and thermal hyperalgesia in mice, providing confidence in specificity. GIPC1 siRNA similarly prevents NGF-induced nociception. NRP1 and GIPC1 inhibition blunts inflammatory nociception, indicating that NRP1 and GIPC1 mediate the nociceptive action of endogenous and exogenous NGF. NRP1 is necessary for NGF-induced action potential firing in both mouse and human DRG neurons, supporting human translation. NRP1 is required for the proximal events of NGF-evoked nociception (TrkA dimerization, phosphorylation, channel activation), as well as sustained components of pain signaling (ERK activation, transcription), both of which mediate nociceptor sensitization (50). Although TrkA is the principal pronociceptive NGF receptor, $p75^{NTR}$ also contributes to NGF-induced pain (51) and the effect of NRP1 on $p75^{NTR}$ warrants further study. NGF/TrkA signalosomes transported from nerve terminals to the soma have been studied in compartmentalized sympathetic (52) and DRG (53) neuronal cultures, where retrograde NGF/TrkA signaling controls gene expression during the development of sympathetic neurons. Whether endosomal signaling of NGF/TrkA contributes to pain, as observed with G protein-coupled receptors (54), deserves further attention. Additional studies are also required to determine whether NRP1 is necessary for NGF-induced expression of pronociceptive transmitters and channels, and whether NRP1 mediates the neurotrophic actions of NGF. NRP1 interacts with semaphorins (19) as a co-receptor for plexins, which regulate TrkA retrograde signaling (55). Accordingly, NRP1 is also highly expressed in axonal growth cones (56), as well as small diameter NGF-responsive DRG neurons during neurite sprouting (57). Thus, disruption of NRP1 could affect NGF-induced neuronal growth, with implications for the neuroplasticity associated with chronic pain.

NGF is implicated in neuropathic, surgical and cancer pain (5), highlighting the need to study contributions of NRP1 and GIPC1 across pain pathologies. Upregulation of NRP1 and GIPC1 in painful conditions, such as cancer, could amplify NGF/TrkA signaling. Changes in NRP1 expression have been reported in migraine patients (58); though presumed to link to vasculature changes through VEGF signaling, this could mediate migraine pain through NGF (59). Given the key role of NGF/TrkA in pain and the challenge of developing TrkA-selective antagonists, NGF mAbs were prioritized for the treatment of pain. While NGF mAbs provided beneficial pain relief to patients with arthritis, rapidly progressing osteoarthritis observed in some patients has precluded FDA approval (12). It is unknown whether NRP1 contributes to NGF signaling in bone tissue, considering its expression on osteoblasts (60). Similar to the development of partial or biased drugs that 'fine-tune' G protein-coupled receptor signaling to reduce adverse effects, targeting NGF signaling *via* co-receptors/scaffolds could be advantageous for treating patients that suffer from chronic pain without the side effects of systemic NGF sequestration. Identifying the antinociceptive efficacy of vesencumab highlights an opportunity to repurpose a biologic developed for cancer for the treatment of chronic pain, facilitating the development of a non-opioid therapeutic targeting NGF signaling through this novel co-receptor.

Materials and Methods

See SI for complete Materials and Methods

siRNA. siRNAs were from Dharmacon (**Table S4**).

Animals. New York University Institutional Animal Care and Use Committee approved experiments.

Microscale thermophoresis. Fluorescent NGF was mixed with NRP1 for thermophoresis measurements.

HiBiT-BRET binding assays. SnapTag-NRP1 or SnapTag-NRP1 Y297A were expressed in HEK293T cells and labeled with SNAP-Surface® Alexa Fluor® 488. Separately, IL-6-HiBiT-$VEGF_{165}$a or IL-6-NGF-HiBiT were expressed in other HEK293T cells. Secreted growth factor was collected as cell supernatant. Supernatant was incubated with recombinant HaloTag-LgBiT and nanoluciferase substrate furimazine. NRP1-expressing cells were pre-incubated with vehicle or unlabeled $VEGF_{165}$a, followed by supernatant with furimazine. Luminescence and fluorescence emissions were recorded.

NGF/TrkA/NRP1 computational modeling. Ternary complexes of human NGF/TrkA/NRP1 were generated through an information-driven computational docking protocol (27) and were compared to existing biochemical and molecular data.

Mouse tissue. Anesthetized mice were transcardially perfused with 4% paraformaldehyde. DRG (L4-L5) were fixed in 4% paraformaldehyde, cryoprotected, embedded, and sectioned.

Human tissue. Collection of DRG from deidentified organ donors was reviewed by the Institutional Review Board of the University of Cincinnati (#00003152, Study ID 2015-5302) and deemed to be human subjects exempt. Donor information has been provided (61). DRG (L4-L5) were fixed in 4% paraformaldehyde, cryoprotected, embedded, and sectioned.

Immunofluorescence. Sections were incubated with primary antibodies to TrkA, NRP1, CGRP, and P2X3. Slides were washed, incubated with fluorescent secondary antibodies and imaged by confocal microscopy.

RNAScope™ *in situ* hybridization. NRP1, TrkA and GIPC1 were localized by RNAScope™ using probes to mouse and human targets.

DRG culture. Human DRG suspension cells were from AnaBios Corporation and were studied within 96 h. Thoracic and lumbar mouse DRG were enzymatically dissociated. GIPC1 or Ctrl siRNA plus a plasmid encoding the enhanced green fluorescent protein (eGFP) were expressed by Nucleofector® transfection. Neurons were used within 48 h and siRNA transfection verified by eGFP fluorescence.

Patch-clamp. Action potentials were recorded in whole-cell patch clamp configuration and current-clamp mode. Action potentials were evoked by a ramp pulse from 0-1000 pA in 1 sec for human DRG, or 0-250 pA in 1 sec for mouse DRG. Rheobase was measured by injecting currents from 0 pA with an increment of 50 pA in 100 ms (human) or 10 pA in 50 ms (mouse). Ca^{2+} currents (ICa^{2+}) and Na^{+} (INa^{+}) currents were recorded as described (17, 18). DRG neurons were preincubated with EG00229 or vehicle (0.1% DMSO) and then challenged with NGF.

NGF-evoked nociception. Mouse NGF was administered by i.pl. injection into the right hindpaw of mice. EG00229, compound 5 (35), a human monoclonal anti-NRP1 antibody (Vesencumab), or IgG control was administered (i.pl.) concomitantly with NGF.

Inflammatory pain. CFA or vehicle (0.9% NaCl) was administered (i.pl.) into the right hindpaw of mice. NRP1 inhibitors were injected (i.pl.) 48 h after CFA.

Intrathecal siRNA. Mouse GIPC1 or Ctrl siRNA was mixed with *in vivo*-jetPEI transfection reagent and administered to conscious mice (i.t., L4-L5), 48 h before NGF (i.pl.) or 48 h after CFA (i.pl.). *Gipc1* mRNA in DRG (L4-L5) was analyzed by RNAScope™ *in situ* hybridization, 48 h after siRNA injection.

Nociception assays. Investigators were blinded to treatments. Mechanical allodynia and thermal hyperalgesia were measured (61).

TrkA phosphorylation. Activated TrkA was detected in cultured DRG neurons by immunofluorescence using a rabbit mAb to phosphorylated TrkA Y785/TrkB Y816.

ERK activity and ERK transcriptional activity. ERK activity was measured in cells expressing EKAR FRET biosensors. ERK transcriptional activity was measured in cells expressing SRE-Luc2P biosensors.

Live cell imaging. Cells expressing SnapTag-TrkA and HaloTag-NRP1 were labeled with membrane-impermeant SNAP-Surface® Alexa Fluor® 488 and membrane-impermeant HaloTag® Alexa Fluor® 660 and were imaged.

Receptor-receptor BRET. For end point studies, HEK293T cells were transfected with a fixed concentration of NanoLuc-NRP1, NanoLuc-p75^{NTR} or NanoLuc-TrkA and increasing concentrations of SnapTag-TrkA or SnapTag-CALCRL. For kinetic studies, cells were transfected with NanoLuc-TrkA, SnapTag-TrkA and either pcDNA3.1 or HaloTag-NRP1. Cells were incubated with SNAP-Surface® Alexa Fluor® 488. Luminescence and fluorescence were measured.

Quantifying SNAP-Surface® Alexa Fluor® 488. HEK293T or CAD.a cells were transfected with SnapTag-TrkA and pcDNA3.1 or HaloTag-NRP1. Cells were labeled using SNAP-Surface® Alexa Fluor® 488 and HaloTag® Alexa Fluor® 660, washed and fluorescence emissions were recorded.

BRET trafficking. Cells were transfected with TrkA-HA-Rluc8 and fluorescent markers for the plasma membrane (RGFP-CAAX), early endosomes (tdRGFP-Rab5a), recycling endosomes (tdRGFP-Rab4a) or cis-Golgi apparatus (tdRGFP-Giantin). In some conditions, cells were co-transfected with pcDNA3.1 or HaloTag-NRP1, or siRNA. Cells were preincubated with hypertonic sucrose, clathrin inhibitor pitstop 2, GIPC1 inhibitor CR1023 or its negative control (CR2055), or myosin VI inhibitor TIP. Cells were incubated with luciferase substrate coelenterazine purple and stimulated with NGF. BRET ratios were recorded.

Quantitative PCR (qPCR). Primers to hTrkA (Hs01021011_m1), mTrkA (Mm01219406_m1), hNgfr (Hs00609976_m1), mNgfr (Mm00446296_m1), hGIPC1 (Hs00991802_m1), mGIPC1 (Mm00457561_m1), or GAPDH (Mn99999915_g1) were used. The relative abundance of mRNA was calculated (61).

Data analysis. Data presented as mean ± SEM. Differences were assessed using paired or unpaired t-test for two comparisons, and 1- or 2-way ANOVA and Tukey's, Dunnett's or Šidák's post-hoc test for multiple comparisons. $P<0.05$ was considered significant at the 95% confidence level.

Acknowledgments. CJP was funded by the Leon Levy Fellowship in Neuroscience (CP, 2022-2023). Supported by grants from: National Institutes of Health (NS102722, DK118971, DE026806, DE029951, RM1DE033491 (NWB, BLS), GM147088 (ARBT), GM133598 (AdG), NS098772, NS120663, DA042852 (RK), NS134965 (KG) and Department of Defense (W81XWH1810431, W81XWH2210239, NWB, BLS). We thank Laura Kilpatrick and Stephen Hill from the University of Nottingham, and Promega Corporation for NRP1 cDNA plasmids. We thank Paz Durán for CAD.a cells.

References

1. R. Levi-Montalcini, V. Hamburger, Selective growth stimulating effects of mouse sarcoma on the sensory and sympathetic nervous system of the chick embryo. *J Exp Zool* **116**, 321-361 (1951).
2. R. Klein, S. Q. Jing, V. Nanduri, E. O'Rourke, M. Barbacid, The trk proto-oncogene encodes a receptor for nerve growth factor. *Cell* **65**, 189-197 (1991).

3. M. Ye, K. M. Lehigh, D. D. Ginty, Multivesicular bodies mediate long-range retrograde NGF-TrkA signaling. *Elife* **7** (2018).
4. M. L. Grimes, E. Beattie, W. C. Mobley, A signaling organelle containing the nerve growth factor-activated receptor tyrosine kinase, TrkA. *Proc Natl Acad Sci U S A* **94**, 9909-9914 (1997).
5. F. Denk, D. L. Bennett, S. B. McMahon, Nerve Growth Factor and Pain Mechanisms. *Annual Review of Neuroscience* **40**, 307-325 (2017).
6. S. P. Banerjee, S. H. Snyder, P. Cuatrecasas, L. A. Greene, Binding of nerve growth factor receptor in sympathetic ganglia. *Proc Natl Acad Sci U S A* **70**, 2519-2523 (1973).
7. D. Johnson *et al.*, Expression and structure of the human NGF receptor. *Cell* **47**, 545-554 (1986).
8. B. L. Hempstead, D. Martin-Zanca, D. R. Kaplan, L. F. Parada, M. V. Chao, High-affinity NGF binding requires coexpression of the trk proto-oncogene and the low-affinity NGF receptor. *Nature* **350**, 678-683 (1991).
9. Y. Indo *et al.*, Mutations in the TRKA/NGF receptor gene in patients with congenital insensitivity to pain with anhidrosis. *Nat Genet* **13**, 485-488 (1996).
10. E. Einarsdottir *et al.*, A mutation in the nerve growth factor beta gene (NGFB) causes loss of pain perception. *Hum Mol Genet* **13**, 799-805 (2004).
11. N. E. Lane *et al.*, Tanezumab for the treatment of pain from osteoarthritis of the knee. *N Engl J Med* **363**, 1521-1531 (2010).
12. M. C. Hochberg *et al.*, When Is Osteonecrosis Not Osteonecrosis?: Adjudication of Reported Serious Adverse Joint Events in the Tanezumab Clinical Development Program. *Arthritis Rheumatol* **68**, 382-391 (2016).
13. P. Ray *et al.*, Comparative transcriptome profiling of the human and mouse dorsal root ganglia: an RNA-seq-based resource for pain and sensory neuroscience research. *Pain* **159**, 1325-1345 (2018).
14. M. Broz, A. Kolarič, M. Jukič, U. Bren, Neuropilin (NRPs) Related Pathological Conditions and Their Modulators. *International Journal of Molecular Sciences* **23**, 8402 (2022).
15. S. Soker, S. Takashima, H. Q. Miao, G. Neufeld, M. Klagsbrun, Neuropilin-1 is expressed by endothelial and tumor cells as an isoform-specific receptor for vascular endothelial growth factor. *Cell* **92**, 735-745 (1998).
16. Y. Xin *et al.*, Pharmacokinetic and pharmacodynamic analysis of circulating biomarkers of anti-NRP1, a novel antiangiogenesis agent, in two phase I trials in patients with advanced solid tumors. *Clin Cancer Res* **18**, 6040-6048 (2012).
17. A. Moutal *et al.*, SARS-CoV-2 spike protein co-opts VEGF-A/neuropilin-1 receptor signaling to induce analgesia. *Pain* **162**, 243-252 (2021).
18. K. Gomez *et al.*, Neuropilin-1 is essential for vascular endothelial growth factor A-mediated increase of sensory neuron activity and development of pain-like behaviors. *Pain* 10.1097/j.pain.0000000000002970 (2023).
19. A. L. Kolodkin *et al.*, Neuropilin is a semaphorin III receptor. *Cell* **90**, 753-762 (1997).
20. T. Teesalu, K. N. Sugahara, V. R. Kotamraju, E. Ruoslahti, C-end rule peptides mediate neuropilin-1-dependent cell, vascular, and tissue penetration. *Proc Natl Acad Sci U S A* **106**, 16157-16162 (2009).
21. A. Nykjaer *et al.*, Sortilin is essential for proNGF-induced neuronal cell death. *Nature* **427**, 843-848 (2004).
22. K. S. Sheffield, A. E. Kennedy, J. A. Scott, G. M. Ross, Characterizing nerve growth factor-p75(NTR) interactions and small molecule inhibition using surface plasmon resonance spectroscopy. *Anal Biochem* **493**, 21-26 (2016).
23. M. Teran, M. A. Nugent, Characterization of receptor binding kinetics for vascular endothelial growth factor-A using SPR. *Anal Biochem* **564-565**, 21-31 (2019).
24. Q. Pan *et al.*, Neuropilin-1 binds to VEGF121 and regulates endothelial cell migration and sprouting. *J Biol Chem* **282**, 24049-24056 (2007).
25. A. Jarvis *et al.*, Small molecule inhibitors of the neuropilin-1 vascular endothelial growth factor A (VEGF-A) interaction. *J Med Chem* **53**, 2215-2226 (2010).

26. C. J. Peach *et al.*, Real-Time Ligand Binding of Fluorescent VEGF-A Isoforms that Discriminate between VEGFR2 and NRP1 in Living Cells. *Cell Chem Biol* **25**, 1208-1218 e1205 (2018).
27. G. C. P. van Zundert *et al.*, The HADDOCK2.2 Web Server: User-Friendly Integrative Modeling of Biomolecular Complexes. *Journal of Molecular Biology* **428**, 720-725 (2016).
28. T. Yelland, S. Djordjevic, Crystal Structure of the Neuropilin-1 MAM Domain: Completing the Neuropilin-1 Ectodomain Picture. *Structure* **24**, 2008-2015 (2016).
29. T. Wehrman *et al.*, Structural and mechanistic insights into nerve growth factor interactions with the TrkA and p75 receptors. *Neuron* **53**, 25-38 (2007).
30. B. J. C. Janssen *et al.*, Neuropilins lock secreted semaphorins onto plexins in a ternary signaling complex. *Nature Structural & Molecular Biology* **19**, 1293-1299 (2012).
31. M. W. Parker, P. Xu, X. Li, C. W. Vander Kooi, Structural Basis for Selective Vascular Endothelial Growth Factor-A (VEGF-A) Binding to Neuropilin-1*. *Journal of Biological Chemistry* **287**, 11082-11089 (2012).
32. C. W. Vander Kooi *et al.*, Structural basis for ligand and heparin binding to neuropilin B domains. *Proc Natl Acad Sci U S A* **104**, 6152-6157 (2007).
33. F. L. Watson, M. A. Porcionatto, A. Bhattacharyya, C. D. Stiles, R. A. Segal, TrkA glycosylation regulates receptor localization and activity. *Journal of Neurobiology* **39**, 323-336 (1999).
34. D. Lu, G. Shang, X. He, X.-c. Bai, X. Zhang, Architecture of the Sema3A/PlexinA4/Neuropilin tripartite complex. *Nature Communications* **12**, 3172 (2021).
35. S. Perez-Miller *et al.*, Novel Compounds Targeting Neuropilin Receptor 1 with Potential To Interfere with SARS-CoV-2 Virus Entry. *ACS Chem Neurosci* **12**, 1299-1312 (2021).
36. Y. Qi, J. K. Wang, M. McMillian, D. M. Chikaraishi, Characterization of a CNS cell line, CAD, in which morphological differentiation is initiated by serum deprivation. *J Neurosci* **17**, 1217-1225 (1997).
37. C. J. Peach, L. E. Kilpatrick, J. Woolard, S. J. Hill, Use of NanoBiT and NanoBRET to monitor fluorescent VEGF-A binding kinetics to VEGFR2/NRP1 heteromeric complexes in living cells. *Br J Pharmacol* **178**, 2393-2411 (2021).
38. Y. Namkung *et al.*, Monitoring G protein-coupled receptor and β-arrestin trafficking in live cells using enhanced bystander BRET. *Nature Communications* **7**, 12178 (2016).
39. H. Cai, R. R. Reed, Cloning and characterization of neuropilin-1-interacting protein: a PSD-95/Dlg/ZO-1 domain-containing protein that interacts with the cytoplasmic domain of neuropilin-1. *J Neurosci* **19**, 6519-6527 (1999).
40. X. Lou, H. Yano, F. Lee, M. V. Chao, M. G. Farquhar, GIPC and GAIP form a complex with TrkA: a putative link between G protein and receptor tyrosine kinase pathways. *Mol Biol Cell* **12**, 615-627 (2001).
41. S. N. Naccache, T. Hasson, A. Horowitz, Binding of internalized receptors to the PDZ domain of GIPC/synectin recruits myosin VI to endocytic vesicles. *Proc Natl Acad Sci U S A* **103**, 12735-12740 (2006).
42. M. H. Muders *et al.*, Targeting GIPC/synectin in pancreatic cancer inhibits tumor growth. *Clin Cancer Res* **15**, 4095-4103 (2009).
43. S. M. Heissler *et al.*, Kinetic properties and small-molecule inhibition of human myosin-6. *FEBS Lett* **586**, 3208-3214 (2012).
44. B. Herzog, C. Pellet-Many, G. Britton, B. Hartzoulakis, I. C. Zachary, VEGF binding to NRP1 is essential for VEGF stimulation of endothelial cell migration, complex formation between NRP1 and VEGFR2, and signaling via FAK Tyr407 phosphorylation. *Mol Biol Cell* **22**, 2766-2776 (2011).
45. M. M. Martino, P. S. Briquez, A. Ranga, M. P. Lutolf, J. A. Hubbell, Heparin-binding domain of fibrin(ogen) binds growth factors and promotes tissue repair when incorporated within a synthetic matrix. *Proc Natl Acad Sci U S A* **110**, 4563-4568 (2013).
46. D. Mahadeo, L. Kaplan, M. V. Chao, B. L. Hempstead, High affinity nerve growth factor binding displays a faster rate of association than p140trk binding. Implications for multi-subunit polypeptide receptors. *J Biol Chem* **269**, 6884-6891 (1994).

47. X. L. He, K. C. Garcia, Structure of nerve growth factor complexed with the shared neurotrophin receptor p75. *Science* **304**, 870-875 (2004).
48. D. C. Lin *et al.*, APPL1 associates with TrkA and GIPC1 and is required for nerve growth factor-mediated signal transduction. *Mol Cell Biol* **26**, 8928-8941 (2006).
49. S. Koch *et al.*, NRP1 presented in trans to the endothelium arrests VEGFR2 endocytosis, preventing angiogenic signaling and tumor initiation. *Dev Cell* **28**, 633-646 (2014).
50. M. Malik-Hall, O. A. Dina, J. D. Levine, Primary afferent nociceptor mechanisms mediating NGF-induced mechanical hyperalgesia. *Eur J Neurosci* **21**, 3387-3394 (2005).
51. K. Sung *et al.*, Swedish Nerve Growth Factor Mutation (NGF(R100W)) Defines a Role for TrkA and p75(NTR) in Nociception. *J Neurosci* **38**, 3394-3413 (2018).
52. R. Kuruvilla, H. Ye, D. D. Ginty, Spatially and functionally distinct roles of the PI3-K effector pathway during NGF signaling in sympathetic neurons. *Neuron* **27**, 499-512 (2000).
53. J. D. Delcroix *et al.*, NGF signaling in sensory neurons: evidence that early endosomes carry NGF retrograde signals. *Neuron* **39**, 69-84 (2003).
54. D. D. Jensen *et al.*, Neurokinin 1 receptor signaling in endosomes mediates sustained nociception and is a viable therapeutic target for prolonged pain relief. *Sci Transl Med* **9** (2017).
55. N. Yamashita, M. Yamane, F. Suto, Y. Goshima, TrkA mediates retrograde semaphorin 3A signaling through plexin A4 to regulate dendritic branching. *J Cell Sci* **129**, 1802-1814 (2016).
56. A. Estrada-Bernal *et al.*, Functional complexity of the axonal growth cone: a proteomic analysis. *PLoS One* **7**, e31858 (2012).
57. J. N. Reza, I. Gavazzi, J. Cohen, Neuropilin-1 is expressed on adult mammalian dorsal root ganglion neurons and mediates semaphorin3a/collapsin-1-induced growth cone collapse by small diameter sensory afferents. *Mol Cell Neurosci* **14**, 317-326 (1999).
58. P. Gormley *et al.*, Meta-analysis of 375,000 individuals identifies 38 susceptibility loci for migraine. *Nat Genet* **48**, 856-866 (2016).
59. P. Sarchielli, V. Gallai, Nerve growth factor and chronic daily headache: a potential implication for therapy. *Expert Rev Neurother* **4**, 115-127 (2004).
60. J. Harper, L. C. Gerstenfeld, M. Klagsbrun, Neuropilin-1 expression in osteogenic cells: down-regulation during differentiation of osteoblasts into osteocytes. *J Cell Biochem* **81**, 82-92 (2001).
61. R. Tonello *et al.*, The contribution of endocytosis to sensitization of nociceptors and synaptic transmission in nociceptive circuits. *Pain* **164**, 1355-1374 (2023).

Figures

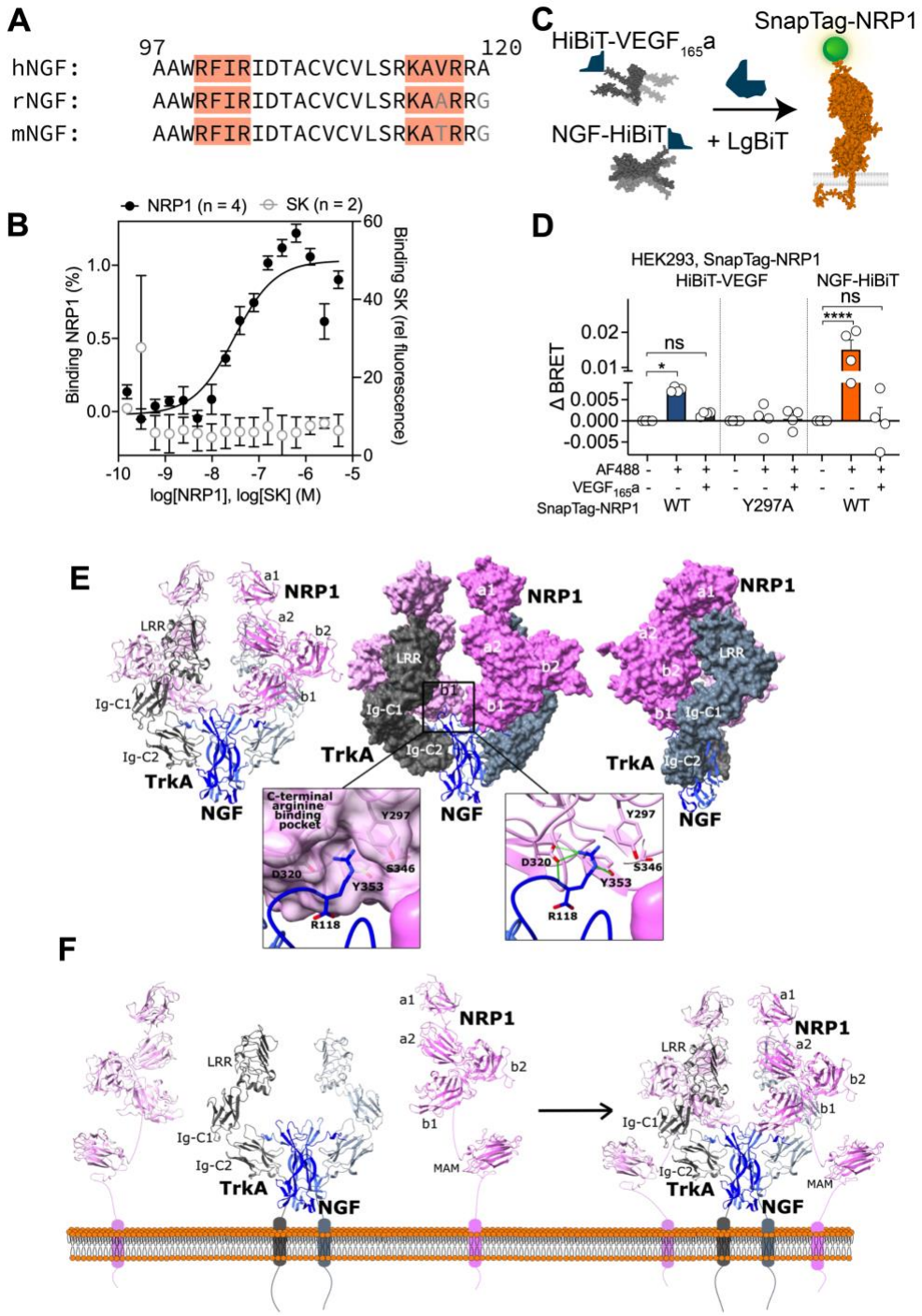

Figure 1. NGF interacts with NRP1. A. Carboxy-terminal sequences of NGF, highlighting prospective CendR motifs (R/KxxR/K). Amino acids numbered according to the mature βNGF sequence (1-120 equivalent to proNGF 122-241). *h, Homo sapiens; r, Rattus norvegicus; m, Mus musculus*. **B.** Interaction between fluorescent human βNGF and human NRP1 (residues 22-644) or staphylokinase (SK, negative control) and using MST. Data from 4 (NRP1) or 2 (SK) independent experiments. Mean±SEM. **C, D.** BRET measurements of VEGF and NGF proximity (<10 nm) to

full-length NRP1 in living HEK293T cells at 37ºC (**C**). Supernatant was collected from cells secreting growth factor ($VEGF_{165}a$ or NGF) tagged with HiBiT, a small fragment of nanoluciferase. When reconstituted with recombinant LgBiT and luciferase substrate, this acts as a bioluminescent donor for SnapTag-NRP1 labeled with SNAPTag-Alexa Fluor® 488 (AF488). BRET was compared to negative control (HiBiT/LgBiT only lacking AF488). Cells were pre-incubated with vehicle or 10 nM unlabeled $VEGF_{165}a$ (30 min), followed by luminescent growth factor (15 min, 37ºC). BRET with HiBiT-$VEGF_{165}a$ was measured between HiBiT-$VEGF_{165}a$ and either SnapTag-NRP1 (WT) or the known $VEGF_{165}a$ binding-dead mutant (Y297A), as well as HiBiT-tagged NGF (**D**). Data from 4 independent experiments with triplicate wells. Mean±SEM. $^{*}P<0.05$, $^{****}P<0.0001$, ns not significant. 1-way ANOVA, Šídák's multiple comparisons. **E, F.** Ternary complex of human NGF/TrkA/NRP1 generated using a data constraint-driven computational docking protocol. Cartoon and surface representation of TrkA (grey shades), NGF (blue shades) and NRP1 (pink shades) are shown. **E.** NGF/TrkA/NRP1 docked model and conserved molecular interactions at the NGF/NRP1 interface. The docked model of NGF/TrkA/NRP1 suggests a 2:2:2 stoichiometry with one NRP1 molecule interacting with one TrkA molecule and the NGF dimer. Two views of the docked complex with NRP1 and TrkA in surface representation are shown to represent shape complementarity between NRP1 and TrkA. Binding of NGF C-terminal R118 (blue sticks) to conserved residues (pink sticks, Y297, D320, S346, Y353) in C-terminal arginine binding pocket located in NRP1 b1 domain is shown as inset with predicted hydrogen bonding interactions depicted as green dashes. **F.** Illustration of the proposed complex formation between NRP1 and NGF/TrkA as it would appear on the cell surface. The membrane proximal MAM domains of NRP1 (PDB 5L73) are included for completeness (MAM domains were not part of docking calculations) to propose a sterically feasible membrane tethered NGF/TrkA/NRP1 complex formation on the cell surface. The membrane linkers connecting NRP1 b2 and MAM domains, linkers connecting NRP1, TrkA with their respective transmembrane regions and the transmembrane regions are not derived from structured components and are not to scale.

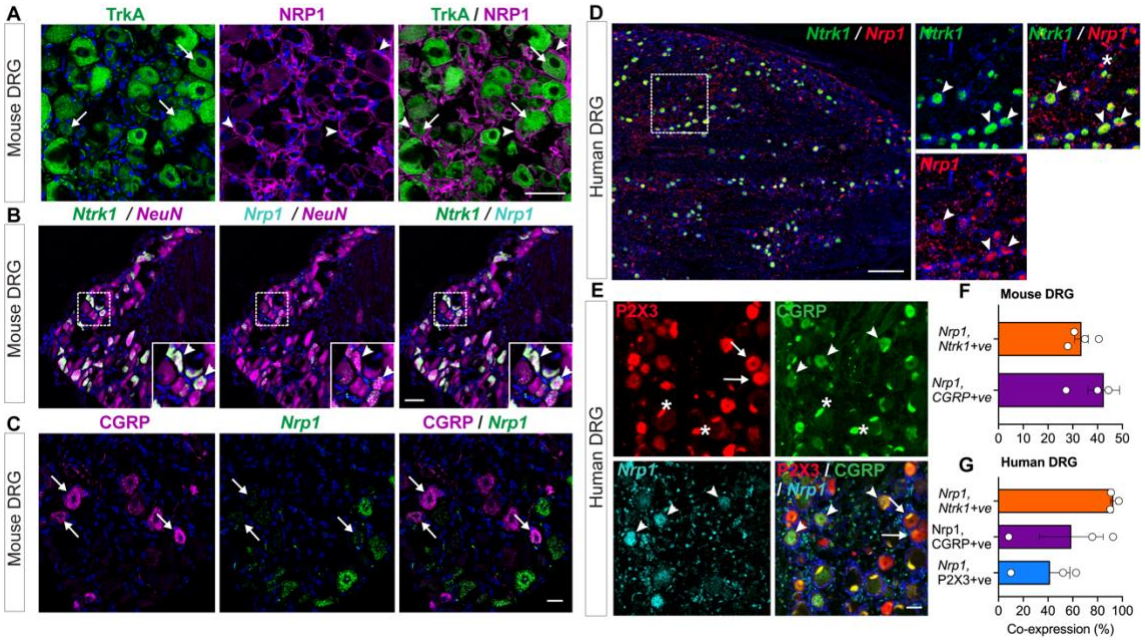

Figure 2. TrkA and NRP1 are coexpressed in DRG. A. Immunofluorescence detection of TrkA and NRP1 in mouse DRG. TrkA was largely intracellular (arrows) whereas NRP1 was detected at the plasma membrane (arrow heads). Scale bar, 50 µm. **B.** RNAScope™ detection of *Ntrk1* (TrkA) and *Nrp1* (NRP1) mRNA in mouse DRG neurons identified by NeuN immunofluorescence. Arrow heads indicate neurons coexpressing *Ntrk1* and *Nrp1*. Scale bar, 50 µm. **C.** Immunofluorescence of CGRP and RNAScope™ detection of *Nrp1* mRNA in mouse DRG. Arrows indicate neurons coexpressing CGRP and *Nrp1*. Scale bar, 20 µm. **D.** RNAScope™ detection of *Ntrk1* and *Nrp1* mRNA in human DRG. Arrow heads indicate neurons coexpressing *Ntrk1* and *Nrp1*. Scale bar, 500 µm. **E.** Immunofluorescence of P2X3 and CGRP and RNAScope™ detection of *Nrp1* mRNA in human DRG. Arrow heads indicate neurons coexpressing CGRP and *Nrp1*. Arrows indicate neurons expressing P2X3 but not *Nrp1*. Scale bar, 50 µm. *Denotes fluorescence in human neurons due to lipofuscin. Nuclei shown in blue. **F.** Percentage of mouse DRG neurons expressing *Ntrk1* or CGRP that coexpress *Nrp1*. **G.** Percentage of human DRG neurons expressing *Ntrk1*, CGRP or P2X3 that coexpress *Nrp1*. A-E show representative images from n=4-5 mice and n=3 humans. F, G show hybridized positive neurons (%) from n=3-4 mice and n=3 humans.

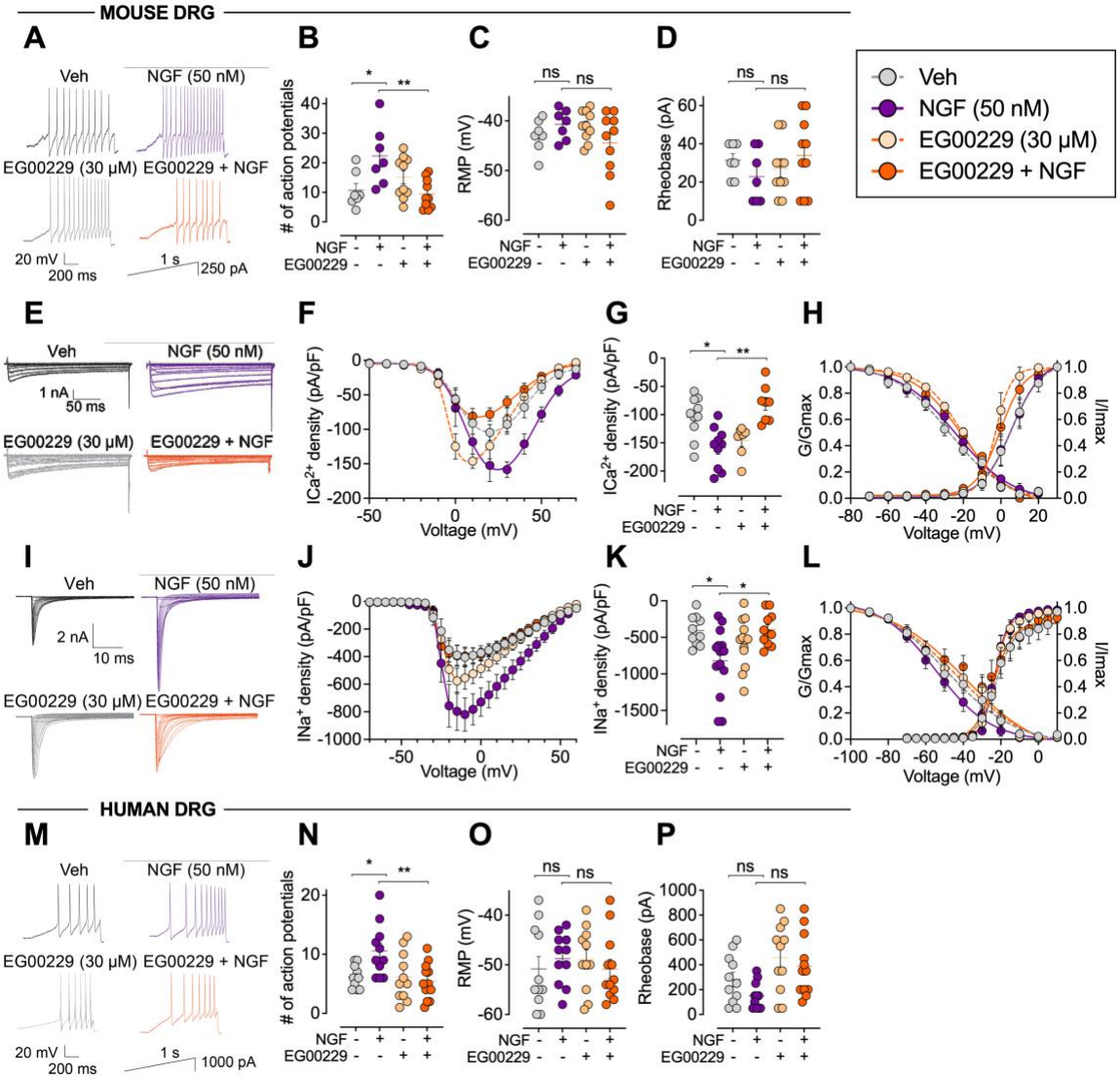

Figure 3. NRP1 inhibition prevents NGF-induced increases in neuronal firing, excitability and ion channel currents. Effect of NRP1 inhibitor EG00229 (30 μM, 30 min) on responses of dissociated mouse (**A-L**) and human (**M-P**) DRG neurons to NGF (50 nM, 30 min). **A, B, M, N.** Representative action potential firing evoked by a depolarizing ramp stimulus (**A, M**), with summary of the number of evoked action potentials (**B, N**). N=7-10 cells. **C, D, O, P.** Resting membrane potential (RMP) (**C, O**) and rheobase (**D, P**). **E-H.** Representative family of Ca^{2+} current traces recorded from small diameter DRG neurons in response to depolarization steps from -70 to +70 mV from a holding potential of -90 mV (**E**), with double Boltzmann fits for current density-voltage curve (**F**), summary of peak calcium current densities (**G**) and Boltzmann fits for voltage-dependence of activation and inactivation (**H**). N=7-10 cells. **I-L.** Representative family of Na^{+} current traces, where currents were evoked by 150 ms pulses between −70 and +60 mV (**I**), with double Boltzmann fits for current density-voltage curve (**J**), summary of peak sodium current densities (**K**) and Boltzmann fits for voltage-dependence of activation and inactivation (**L**). N=10-14 cells. Mean±SEM. *P<0.05, ** P<0.01, ns not significant. B, C, D, G, K, N, O, P. Kruskal-Wallis, Dunn's multiple comparisons.

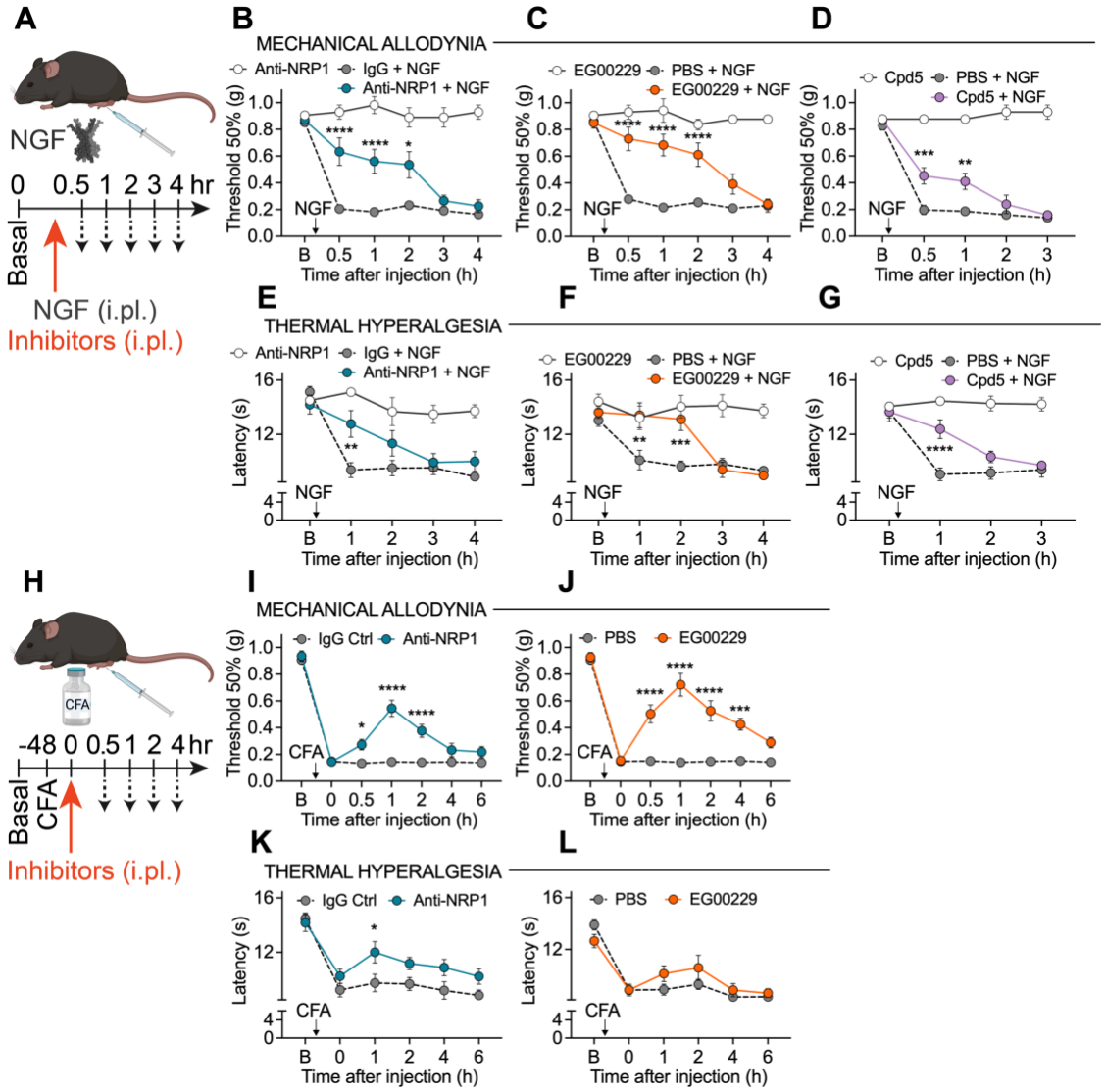

Figure 4. NRP1 inhibition abrogates NGF- and CFA-induced nociception in mice. A-G. NGF-induced nociception. Effects of an antibody against the b1 domain of NRP1 (**B, E**; 7 µg/10 µl i.pl.), or NRP1 inhibitors EG00229 (**C, F**; 30 µM/10 µl i.pl.) or Compound 5 (**D, G**; Cpd5, C,F; 30 µM/10 µl i.pl.). After baseline ("B") measurements, inhibitors were co-injected with murine NGF (50 ng/10 µl, i.pl.). Mechanical allodynia (**B-D**) and thermal hyperalgesia (**E-G**) were measured. n=5-8 mice per group. **H-L.** CFA-induced inflammatory pain. Effects of anti-NRP1 (**I, K**) or EG00229 (**J, L**). Inhibitors were injected (i.pl.) 48 h after CFA (i.pl.). Mechanical allodynia (**I, J**) and thermal hyperalgesia (**K, L**) were measured. n=8-9 mice per group. Mean±SEM. **P*<0.05, ***P*<0.01, ****P*<0.001, *****P*<0.0001 vs. PBS or IgG Ctrl. B-G, I-L. 2-way ANOVA, Sídák's multiple comparisons.

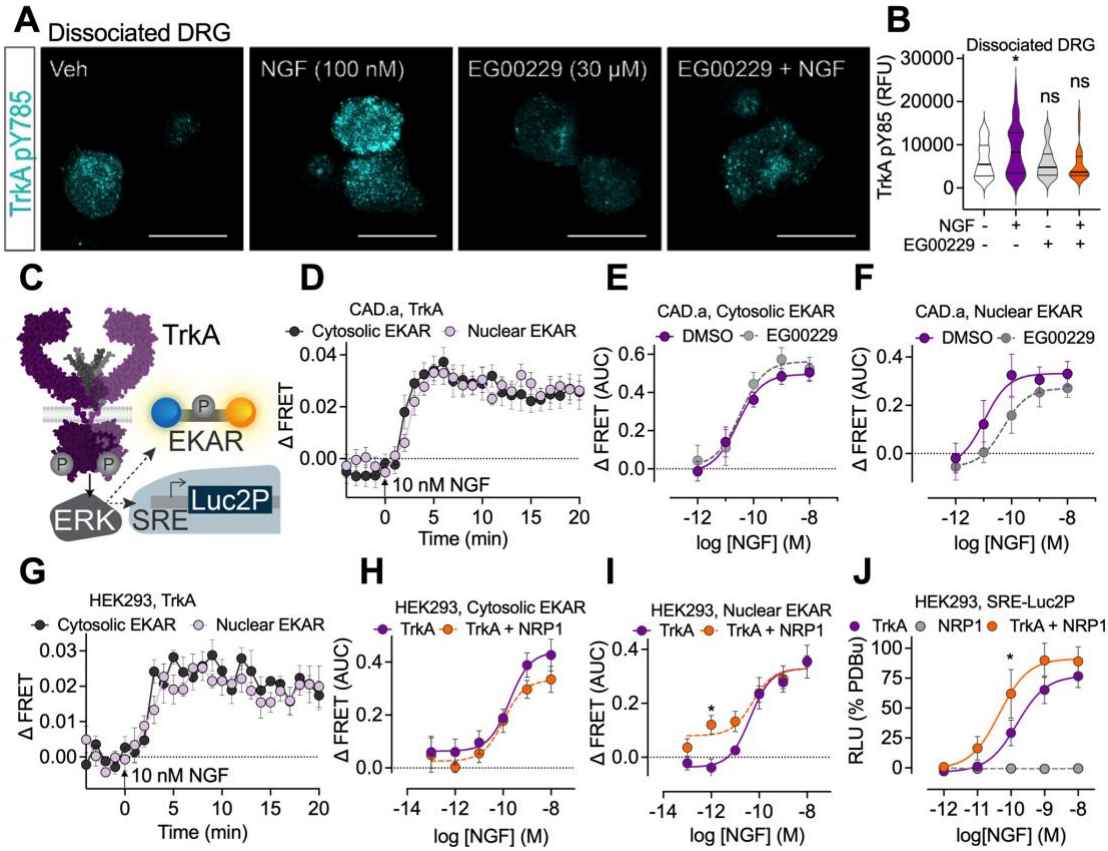

Figure 5. NRP1 modulates TrkA-mediated kinase signaling. A-B. Effect of murine NGF (100 nM, 15 min) and NRP1 inhibitor EG00229 (30 µM, 30 min pre-incubation) on phosphorylated TrkA Y785 staining in mouse DRG neurons. N=34-44 neurons from 3 independent experiments. Scale bar, 20 µm. **C-J.** NGF-induced ERK signaling measured using FRET-based EKAR biosensors (**D-I**) or a downstream luciferase reporter (**J**). **D-I.** NGF-induced modulation of ERK activity using biosensors localized to the cytosol (**D, E**) or nucleus (**D, F**) in neuron-like CAD.a cells expressing human TrkA. Kinetics of NGF-induced ERK monitored in CAD.a cells (**D**), comparing increasing NGF concentrations after pre-incubation with EG00229 (30 µM, 30 min) (**E-F**). **G-I.** ERK signaling in HEK293T cells expressing TrkA alone or expressing both TrkA and NRP1 (**H, I**). **J.** Effect of increasing NGF concentrations on ERK transcription in cells expressing TrkA, NRP1 or both (% positive control, 10 µM PDBu). RFU, relative fluorescence units. AUC, area under curve. RLU, relative luminescence units. Data from 4-8 independent experiments with triplicate wells. Mean±SEM. **P*<0.05, ****P*<0.001, *****P*<0.0001. B, I, J. 1-way ANOVA, Sídák's multiple comparisons.

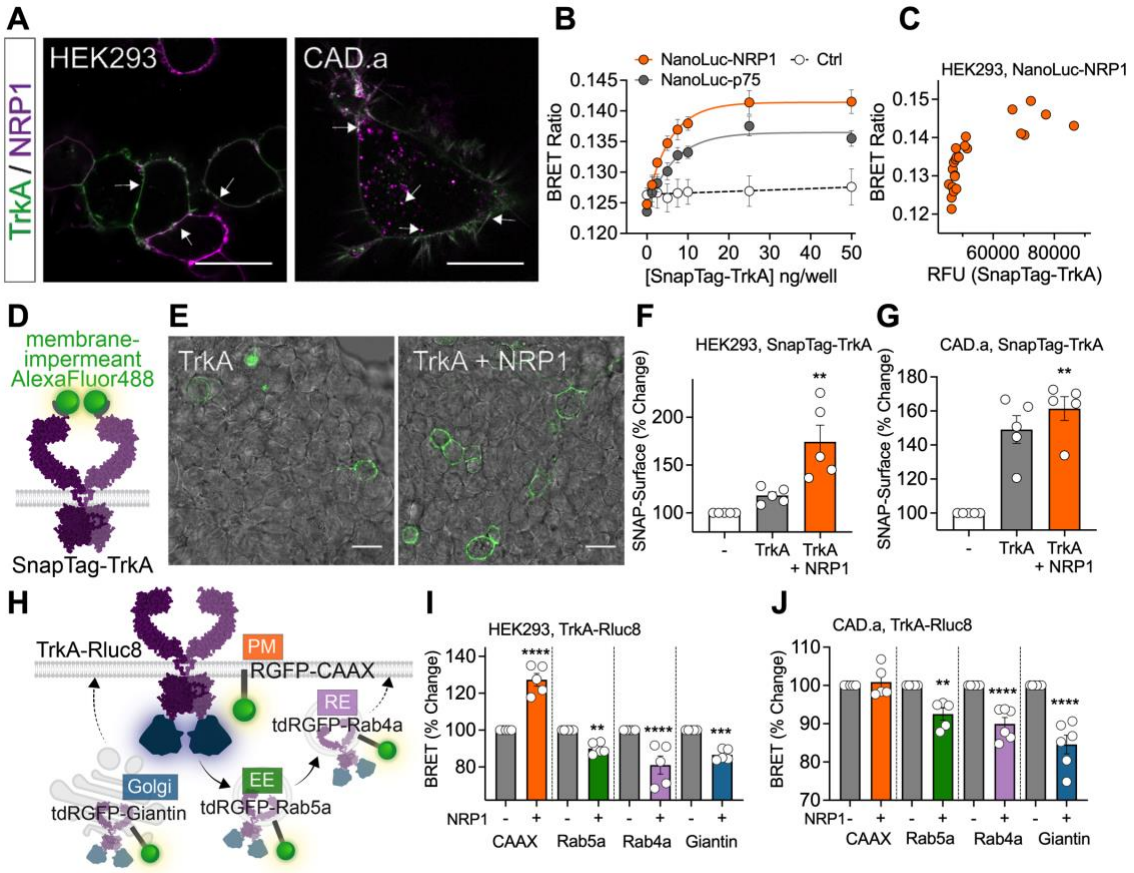

Figure 6. TrkA and NRP1 form a heteromeric complex. **A.** HEK293T or CAD.a cells expressing SnapTag-TrkA and HaloTag-NRP1 simultaneously labeled with membrane-impermeant substrate (SNAPTag-Alexa Fluor® 488, HaloTag-Alexa Fluor® 660). Representative images from n=5 independent experiments. **B, C**. BRET assays to monitor proximity between NanoLuc-NRP1 or NanoLuc-p75^{NTR} and increasing SnapTag-TrkA DNA. Negative control, NanoLuc-TrkA and SnapTag-CALCRL. Representative replicate (**C**) plotting BRET against relative fluorescence units (RFU). **D-G.** Cell-surface TrkA in HEK293T imaged in the absence or presence of NRP1 (**E**). **F-G.** Quantified fluorescence without receptor (-), SnapTag-TrkA alone or SnapTag-TrkA co-transfected with NRP1 in HEK293T (**F**) or CAD.a (**G**) cells. **H-J.** BRET between TrkA tagged with *Renilla* luciferase (Rluc8) and *Renilla* green fluorescent protein (RGFP) tagged markers of the plasma membrane (PM, RGFP-CAAX), early endosome (EE, tdRGFP-Rab5a), recycling endosomes (RE, tdRGFP-Rab4a) or the cis-Golgi apparatus (tdRGFP-Giantin). HEK293T cells (**I**) or CAD.a cells (**J**) were transfected with TrkA-Rluc8 in the absence (-) or presence (+) of NRP1. BRET was normalized relative to TrkA-Rluc8 alone (100%). Scale bar, 20 µm. Data from 5-6 independent experiments with triplicate wells. Mean±SEM. **P*<0.05, ***P*<0.01, ****P*<0.001, *****P*<0.0001. F, G. Paired t-test. I, J. 1-way ANOVA with Šídák's multiple comparisons.

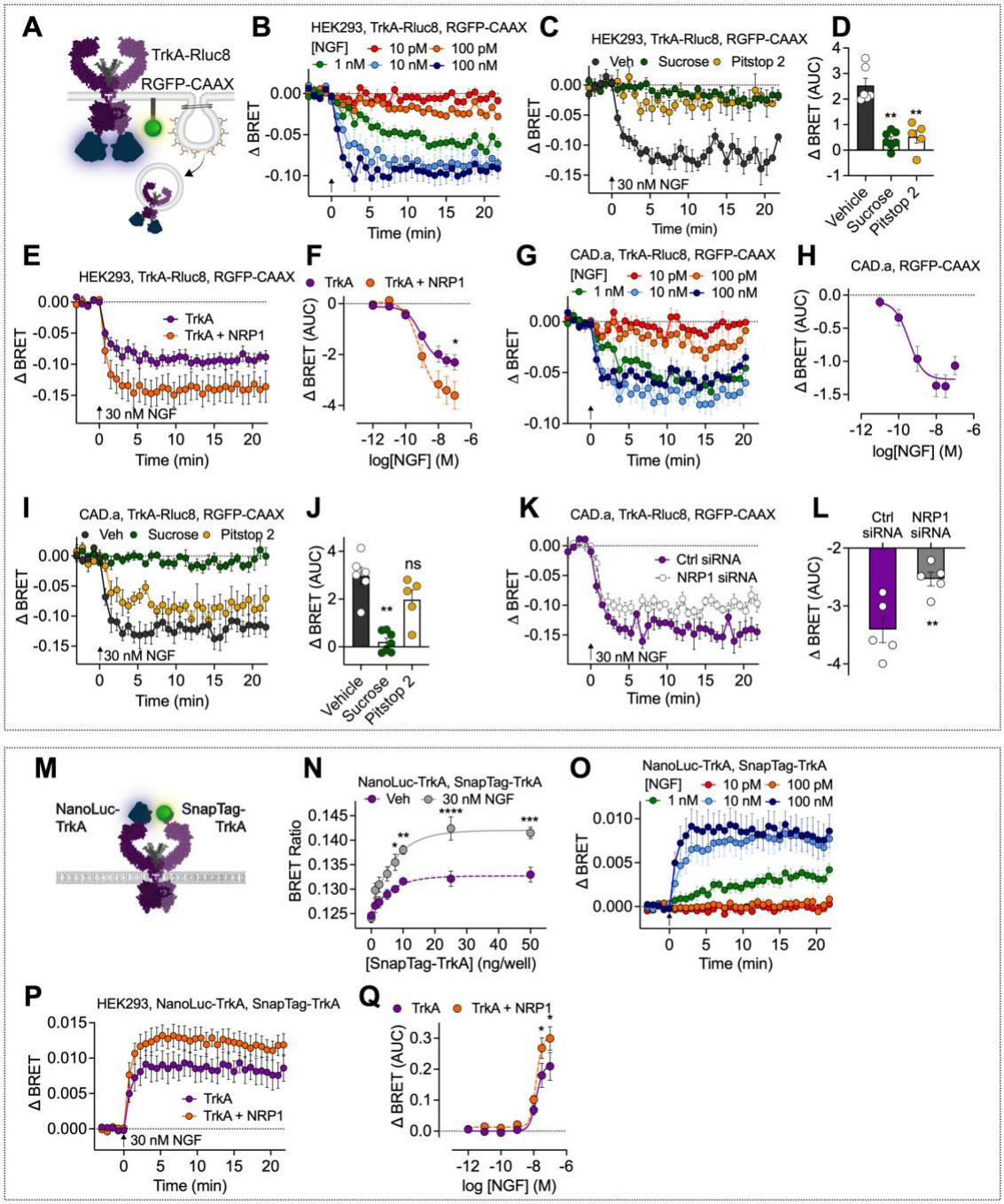

Figure 7. NRP1 modulates NGF-induced TrkA trafficking and RTK oligomerization. **A-L.** BRET measurements between Rluc8-tagged TrkA and a fluorescent marker of the plasma membrane (RGFP-CAAX) at 37°C. Decreased BRET indicates TrkA-Rluc8 removal from the plasma membrane (**A**). **B-F.** Trafficking in HEK293T cells incubated with graded concentrations of NGF (**B**), or pre-incubated for 30 min with hypertonic sucrose (0.45 M), clathrin inhibitor pitstop 2 (30 µM) or vehicle (Veh) (**C, D**) before NGF stimulation. Effect of NRP1 co-expression on NGF-stimulated endocytosis of TrkA (**E, F**). **G-L.** Trafficking in CAD.a cells expressing human TrkA incubated with graded concentrations of NGF (**G, H**), or pre-incubated for 30 min with hypertonic

sucrose (0.45 M), clathrin inhibitor pitstop 2 (30 μM) or vehicle (Veh) (**I, J**) before NGF stimulation, or transfected with control or murine NRP1 siRNA (**K, L**). **M-Q.** BRET measurements between NanoLuc-TrkA and SnapTag-TrkA to assess TrkA oligomerization in HEK293T cells. **N.** BRET with increasing expression of SnapTag-TrkA and fixed NanoLuc-TrkA (10 ng), after 30 min incubation with vehicle or NGF. **O-Q.** Using a fixed donor:acceptor ratio (1:2.5), oligomerization kinetics at 37ºC in response to increasing NGF concentrations (**O**) in the absence and presence of NRP1 co-expression (**P, Q**). AUC, area under curve. Data from 4-6 independent experiments with triplicate wells. Mean±SEM. *P<0.05, **P<0.01, ***P<0.001, ****P<0.0001. G, Unpaired t-test. D, I, K. 1-way ANOVA with Sídák's multiple comparisons.

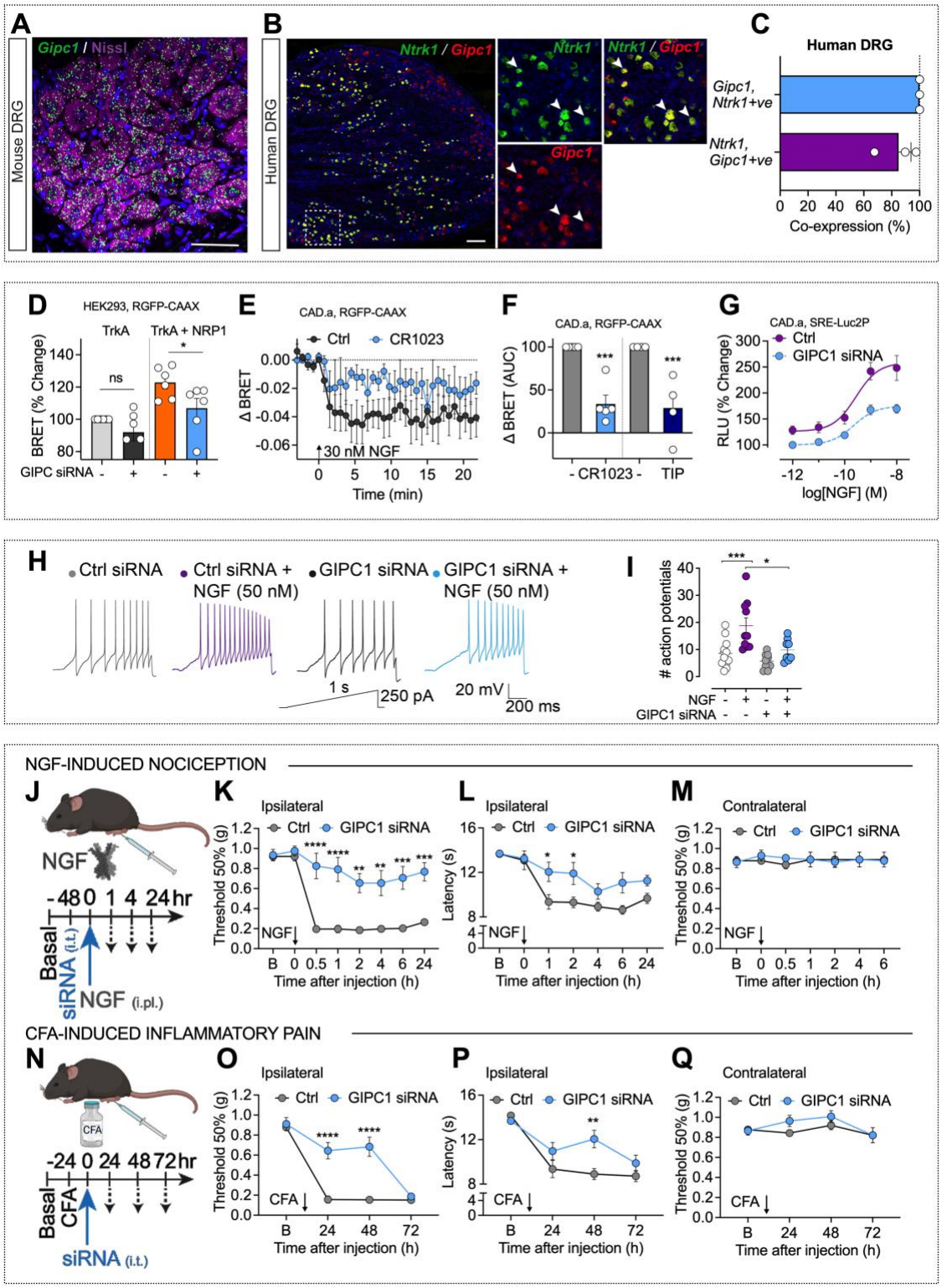

Figure 8. GIPC1 modulates TrkA trafficking, signaling and NGF-induced nociception. A-C. RNAScope™ localization of *Gipc1* mRNA in mouse DRG (**A**) and of *Ntrk1* and *Gipc1* mRNA in human DRG (**B**). Arrows indicate mRNA expression within the same cell. Representative images,

n=5 mice and n=3 humans. Scale bar, 500 µm. C. Percentage of human DRG neurons expressing *Ntrk1 or Gipc1* that coexpress *Gipc1* or *Nrp1*. Hybridized positive neurons (%) from n=3 humans. **D.** Effect of GIPC1 siRNA on BRET measurements of TrkA levels at the plasma membrane of HEK293T cells under basal conditions and after coexpression with NRP1. **E, F.** Effect of 30 min pre-incubation of GIPC1 antagonist (300 µM CR1023 or inactive control, Ctrl) or myosin VI inhibitor (50 µM 2,4,6-Triiodophenol, TIP) on NGF-induced TrkA-Rluc8 trafficking from a marker of the plasma membrane (RGFP-CAAX) in CAD.a cells. **G.** Effect of GIPC1 siRNA on NGF-induced downstream ERK transcription in CAD.a cells. Data from 5-6 independent experiments with triplicate wells. **H, I.** Sample traces of action potential firing in mouse DRG neurons evoked by injecting a 1 s ramp pulse from 0 to 250 pA (**G**), with the number of evoked action potentials (**H**). N=7-10 cells. **J-M.** NGF-induced nociception. Effects of GIPC1 or Ctr siRNA (i.t.) on NGF (50 ng/10 µl, i.pl.)-induced mechanical allodynia (**K**) and thermal hyperalgesia (**L**) in the ipsilateral paw and mechanical allodynia of the contralateral paw (**M**). **N-Q.** CFA-induced nociception. Effects of GIPC1 or Ctr siRNA (i.t.) on CFA (i.pl.)-induced mechanical allodynia (**O**) and thermal hyperalgesia (**P**) in the ipsilateral paw and mechanical allodynia of the contralateral paw (**Q**). N=6-8 mice per group. RLU, relative luminescence units. AUC, area under curve. 'B', basal. Mean±SEM. $P<0.05$, $^{**}P<0.01$, $^{***}P<0.001$, $^{****}P<0.0001$. C,E. 1-way ANOVA, Sídák's multiple comparisons. H, Tukey's multiple comparison. K-M, O-Q, 2-way ANOVA, Sídák's multiple comparisons.

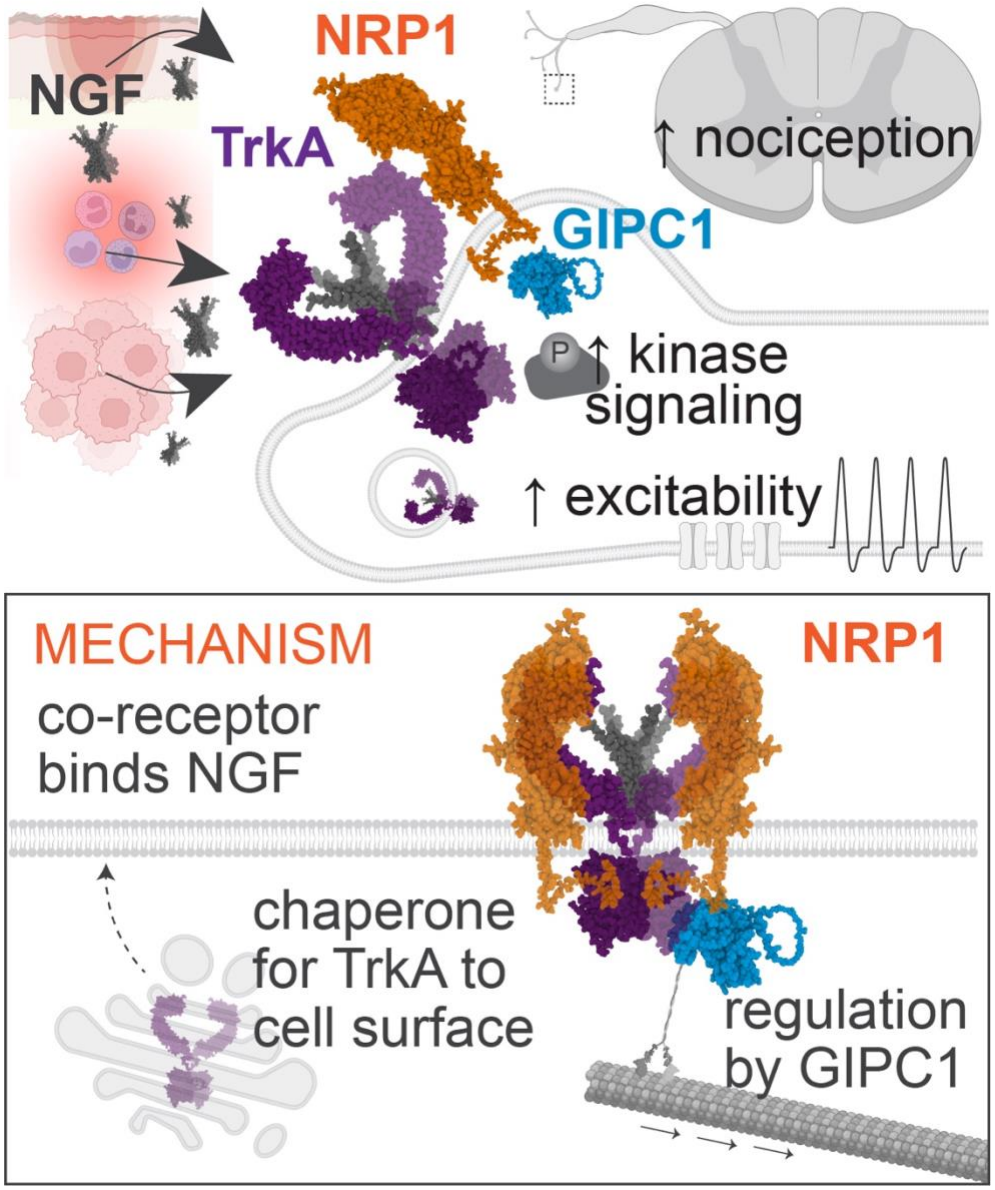

Figure 9. Hypothesized mechanism for NRP1- and GIPC1-mediated NGF/TrkA pain signaling. NGF released from sites of injury, inflammation or the tumor microenvironment binds to and activates TrkA expressed by the peripheral terminals of nociceptors. NRP1 potentiates the actions of NGF in two ways: by directly binding NGF, which enhances TrkA activation; and by chaperoning TrkA from the biosynthetic pathway to the plasma membrane and then signaling endosomes. GIPC1 interacts with both NRP1 and TrkA, which thereby promotes NGF, NRP1 and TrkA-mediated signaling of pain.

Supporting Information for

NEUROPILIN-1 IS A CO-RECEPTOR FOR NGF AND TRKA-EVOKED PAIN

Chloe J. Peach[1,2], Raquel Tonello[1,2], Kimberly Gomez[1,2], Aida Calderon-Rivera[1,2], Renato Bruni[1,2], Harsh Bansia[1,2], Laura Maile[3], Ana-Maria Manu[1,2], Hyunggu Hahn[1,2], Alex R.B. Thomsen[1,2], Brian L. Schmidt[1,2,4,5], Steve Davidson[3], Amedee des Georges[1,2], Rajesh Khanna[1,2,6], *Nigel W. Bunnett[1,2,6]

***Correspondence:** Nigel W. Bunnett, PhD. Room 724, 433 1st Avenue, New York, 10010, USA.
Email: nwb2@nyu.edu

This PDF file includes:

Supporting text SI Materials and Methods
Figures S1 to S4
Tables S1 to S3
SI References

Supporting Information Text

SI Materials and Methods

Reagents. Recombinant βNGF (R&D Systems or Alomone Labs) and recombinant NRP1 (R&D Systems) were reconstituted according to manufacturer's instructions. Unless stated otherwise, *in vitro* studies used human NGF, whereas *ex vivo* and *in vivo* studies used murine NGF. GIPC1 inhibitors (CR1023 or negative control, Ctrl) were from Genscript. Myosin VI inhibitor (2,4,6-triiodophenol) was from Thermo Scientific Chemicals. EG00229 (HY-10799) was from MedChemExpress, compound 5 has been described (1), human monoclonal anti-NRP1 antibody (Vesencumab) was from Invitrogen (MA5-41940), and IgG control (Ctrl) was from ThermoFisher (02-6502).

cDNAs. SnapTag-TrkA was cloned with a GSSGAIA spacer and an N-terminal interleukin-6 signal sequence (IL-6-SnapTag-TrkA). IL-6-NanoLuc-TrkA, IL-6-NanoLuc-p75^{NTR} and TrkA-HA-Rluc8 were cloned using Gibson assembly. HiBiT, a short fragment of NanoLuc (2), was cloned on the N-terminus of VEGF$_{165}$a or C-terminus of βNGF with a GSSG linker. HaloTag-NRP1, SnapTag-NRP1 and NanoLuc-NRP1 were from Dr. Laura Kilpatrick and Prof. Stephen Hill (University of Nottingham). SnapTag-CALCRL was from Alex Thomsen (New York University). RGFP-CAAX (prenylation CAAX box of KRas), tdRGFP-Rab5a, tdRGFP-Rab4a and tdRGFP-Giantin were from M. Bouvier (Université de Montréal). Nuclear and cytosolic EKAR (CFP/YFP) FRET biosensors were from Addgene.

Cell Culture. HEK293T cells were grown in complete Dulbecco's modified Eagle's medium GlutaMAX^{TM} supplemented with 10% fetal bovine serum (FBS) and 100 U/mL penicillin-streptomycin. CAD.a cells were grown in RPMI 1640 containing 4% FBS, 8% horse serum and 100 U/mL penicillin-streptomycin.

siRNAs. ONTARGETplus siRNA targeting human GIPC1 (L-019997-00-0010), murine GIPC1 (L-062534-00-0005) or nontargeting control (Ctrl) siRNA (D-001810-10-05) were from Dharmacon (**Table S3**).

Transfection of cell lines. HEK293T cells were transfected using polyethylenimine (PEI, Polysciences; 1:6 DNA:PEI) diluted in a 150 mM NaCl solution. CAD.a cells were transfected with Lipofectamine 3000 (according to manufacturer's instructions) diluted in serum-free DMEM.

Animals. Experiments were in accordance with the guidelines recommended by the National Institute of Health, the International Association for the study of Pain, the National Centre for the Replacement, Refinement and Reduction of Animals in Research (ARRIVE) guidelines, and were approved by the New York University Institutional Animal Care and Use Committee. Male C57BL/6 mice (8-10 weeks, Charles River) were housed four per cage at 22 ± 0.5°C under a controlled 14/10 h light/dark cycle with free access to food and water. Mice were randomly assigned to experimental groups; group size was based on previous similar studies. Investigators were blind to treatments.

Microscale thermophoresis. Human βNGF (100 µl, 10 µM; R&D Systems Inc.) was fluorescently labeled at lysine residues using the Monolith Protein Labeling Kit RED-NHS 2nd Generation (NanoTemper). Fluorescent NGF (15 nM final) was mixed with increasing concentrations of unlabeled NRP1-His (KactusBio) from 1.5 x 10^{-10} to 5 x 10^{-6} M in MST optimization buffer (50 mM Tris-Cl pH = 7.5, 150 mM NaCl, 10 mM $MgCl_2$, 0.05% Tween-20) and incubated at RT for 30 min. As a negative control, fluorescent NGF (15 nM final) was similarly incubated with staphylokinase from *Staphylococcus aureus* (Genscript). Samples were centrifuged (15,000 g, 10 min) and loaded on MST capillaries. Thermophoresis was measured using a Monolith NT.115 (NanoTemper Technology) at medium MST power. Data from four independent binding experiments was analyzed with GraphPad Prism using a non-linear regression fit (log[agonist] vs response).

HiBiT-BRET binding assay. HEK293T cells were transfected with SnapTag-NRP1 or SnapTag-NRP1 Y297A (3 µg/10 cm dish) using PEI. After 24 h, cells were transferred to 96-well plates. The next day, cells were incubated with SNAP-Surface® Alexa Fluor® 488 (0.25 µM, 1 h, 37ºC), then washed in HBSS/0.1% BSA. Separately, HEK293T cells were transfected with IL-6-HiBiT-VEGF$_{165}$a (3 µg/10 cm dish) or IL-6-NGF-HiBiT (5 µg/dish). After 48 h, medium was replaced with

HBSS/0.1% BSA to collect secreted growth factor in cell supernatant (2 h, 37ºC). Supernatant was diluted (1:2) in HBSS/0.1% BSA and incubated with recombinant HaloTag-LgBiT protein and luciferase substrate furimazine (1:50 final dilution for both; Promega Corporation). NRP1-expressing cells were pre-incubated with vehicle or unlabeled $VEGF_{165}$a (10 nM, 30 min), followed by supernatant with furimazine (1:2, 15 min, 37ºC). Luminescence and fluorescence emissions were recorded (Synergy Neo2, Agilent BioTek; BRET1 donor 460 ± 40 nm, acceptor 540 ± 25 nm).

Information-driven construction of a ternary NGF/TrkA/NRP1 computational model. The TrkA extracellular domain (ECD) structure from the crystal structure of the NGF/TrkA complex (PDB 2IFG) and the AlphaFold (3) -derived model of hNRP1 with only a1a2b1b2 domains were used in docking calculations. hNGF has two prospective 'CendR' R/KxxR/K motifs within the C-terminus that are important for mediating interactions of other growth factors with NRP1 b1 domains (4, 5). The AlphaFold-derived model of soluble hNGF sterically clashed with TrkA when superimposed with the NGF/TrkA crystal structure. Further, the NGF C-terminus $CendR_{118}$ motifs were missing density in NGF/TrkA crystal structure. Hence, Modeller (6) was used to add missing structure to NGF in the NGF/TrkA crystal structure and to sample conformations of NGF $CendR_{118}$ motifs for docking calculations. When modeled on the cell membrane, analysis of the NGF/TrkA crystal structure (PDB 2IFG) revealed that hNGF CendR motif $R_{100}FIR_{103}$ is membrane proximal whereas motif $K_{115}AVR_{118}$ is membrane distal. hNGF polarity with respect to the membrane was determined by the relative membrane orientation of bound hTrkA ECDs (PDB 2IFG). This analysis identified two probable binding modes of NRP1 to the membrane-tethered NGF/TrkA complex. In mode 1, NRP1 b1 domain is poised to interact with CendR motif $R_{100}FIR_{103}$. In this mode, a1a2b2 domains are membrane proximal and NRP1 can possibly interact with the membrane. In mode 2, NRP1 b1 domain is poised to interact with CendR motif $R_{115}FIR_{118}$. This time, the a1a2b2 domains are membrane distal and NRP1 can also possibly interact with the TrkA ECD domains. However, in mode 1, the NGF CendR motif $R_{100}FIR_{103}$ is at the interface with TrkA Ig-C2 domain and is not accessible for NRP1 binding. Hence, we computationally explored binding mode 2 and analyzed its relevance in a physiological context as outlined below.

The NGF/TrkA/NRP1 model was generated in a data-driven approach using HADDOCK 2.4 webserver (7). Since TrkA binding to NGF does not utilize CendR motif $R_{115}FIR_{118}$ of NGF, NRP1 was directly docked to the NGF/TrkA crystal structure. NGF models with solvent-accessible conformations of CendR motif $R_{115}FIR_{118}$ in the NGF/TrkA complex were selected as first docking partners and the AlphaFold-derived NRP1 a1a2b1b2 domain structure as the second docking partner. Knowledge-based restraints in the form of active and passive residues were used as restraints in the docking protocol. In HADDOCK, active residues are solvent-exposed residues directly involved in the interaction between the two proteins followed by solvent-exposed passive residues close to the active residues that may be at the interface (8). From NGF/TrkA, residues of CendR motif $R_{115}FIR_{118}$ and from NRP1, b1 domain residues Y297, D320, S346, T349 and Y353 were specified as active residues. These NRP1 b1 domain residues constitute a C-terminal arginine binding pocket that is known to bind C-terminal arginine in NRP-binding proteins and peptides (4, 5, 9, 10). All residues within 6.5 Å of active residues were specified as passive residues in both docking partners. Standard docking parameters were used during the rigid-body energy minimization followed by semi-flexible refinement where residues at the interface are allowed to move. Besides docking score, several factors were considered while selecting the docked models. This was to ensure the selection of sterically feasible binding modes of NRP1 to NGF/TrkA complex modeled on the membrane without clashing with either the membrane or TrkA. Although non-standard residues were excluded from docking calculations, compatibility of glycosylated TrkA with NRP1 binding in cellular context was considered while selecting docked models (**Fig. S1A**). Further, suitable orientations of the NRP1 b2 domains in connection with NRP1 MAM domain were also considered during selection to ensure membrane-tethered NGF/TrkA/NRP1 complex formation were also possible (**Fig. 1F**). In the different docked poses derived from docking calculations, the NRP1 b1 domain still binds to the NGF C-terminus in a similar manner while NRP1 a1, a2 and b2 domains are oriented differently resulting in poses where one NRP1 molecule can bind to one TrkA monomer (**Fig. 1E**) or two TrkA monomers at once thereby bridging TrkA dimers (**Fig. S1B**) (11). Explicit water refinement was then performed on the selected docked models using the refinement interface of HADDOCK 2.4 webserver (7). The refined ternary complexes were

analyzed for molecular interactions at the interfaces using PISA (12). Structural superposition of structural complexes for analysis and preparation of figures was made using PyMol (13) and UCSF ChimeraX (14).

Collection of mouse tissue. Mice were anesthetized (5% isoflurane) and perfused through the ascending aorta with PBS and then 4% paraformaldehyde in PBS. DRG (L4-L5) were removed, fixed in 4% paraformaldehyde in PBS (1 h, 4°C), cryoprotected in 30% sucrose (24 h, 4°C), and embedded in Optimal Cutting Temperature compound (Tissue Tek). Frozen sections (10-12 µm) were mounted, dried (15 min) and stored (-20°C).

Collection of human tissue. The collection of DRG from deidentified organ donors was reviewed by the Institutional Review Board of the University of Cincinnati (#00003152, Study ID 2015-5302) and deemed to be human subjects exempt. Donor information has been provided (15). DRG (L4-L5) were collected in the operating room within 90 min of aortic cross clamp and after removal of vital organs. DRG were placed in N-methyl-D-glucamine-artificial cerebrospinal fluid (4°C), dissected and immersion fixed in 4% paraformaldehyde in PBS (overnight, 4°C), cryoprotected in 30% sucrose (24 h, 4°C), and embedded in Optimal Cutting Temperature compound. Frozen sections (14-18 µm) were mounted, dried (15 min) and stored (-80°C).

Immunofluorescence. Mouse tissue was blocked (2% bovine serum albumin, BSA, 0.2% Triton X-100 in PBS; 1 h, RT). Sections were incubated (4ºC, overnight) with monoclonal rabbit anti-TrkA (1:50; Millipore-Sigma, SU0354), and monoclonal mouse anti-NRP1 (1:200; Santa Cruz, A-12) or monoclonal human anti-NRP1 vesencumab (1:500; Invitrogen, MA5-41940). Slides were washed and incubated with donkey anti-rabbit Alexa Fluor® 488 (1:1000) and either donkey anti-mouse or anti-human Alexa Fluor® 647 (1:1000, 1 h, RT). Slides were incubated with DAPI (1 µg/ml, 5 min) and mounted (ProLong® Gold Antifade). Sections were imaged using a Leica SP8 confocal microscope with HCX PL APO 10x air objective (Leica Microsystems).

RNAScope™ *in situ* hybridization in mouse and human tissue. mRNA transcripts were localized in mouse and human tissues using a RNAScope™ Multiplex Fluorescent Reagent v2 Assay Kit (Advanced Cell Diagnostics Inc.) using the protocol for fresh-frozen tissue as recommended by the manufacturer, except for omission of the initial on-slide fixation step with mouse tissue. Probes to mouse (Mn) Mm-Nrp1(#471621-C3), Mm-Ntrk1 (#435791-C2), Mm-Gipc1 (#1232971-C1) and human (Hs) Hs-Nrp1 (#424361-C1), Hs-Ntrk1 (#402631-C2) and Hs-Gipc1 (#1232961-C3) were used. Mouse tissue was incubated with Opal 620 (1:1000, FP1495001KT, Akoya Biosciences) and Opal 520 (FP1487001KT) reagents for fluorescence detection. For human tissue, Tyramide Signal Amplification Plus Cyanine 3 (1:1500) and Cyanine 5 (1:1000) were used to detect the hybridized signals. To detect all neurons or peptidergic neurons in mouse tissues, hybridized slides were blocked and incubated with guinea pig anti-NeuN antibody (1:500, EMD Millipore, N90) or rabbit anti-CGRP (1:1000, cat#C8198, Sigma), respectively (overnight, 4°C). Slides were washed and incubated with goat anti-guinea pig Alexa Fluor® 647 (1:1000) or goat anti-rabbit Alexa Fluor® 488 (1:1000, ThermoFisher) (1 hour, RT). Alternatively, neurons were detected using Nissl staining. Slides were washed, incubated with DAPI and mounted. For mouse tissue, sections were imaged using a Leica SP8 confocal microscope with HCX PL APO 40x (NA 1.30) oil objective. The percentage of hybridized positive neurons were quantified and normalized by the total number of neurons. The percentage of hybridized positive peptidergic neurons were quantified and normalized by the total number of peptidergic neurons. To detect peptidergic and non-peptidergic neurons in human tissues, hybridized slides were blocked and incubated with mouse anti-CGRP (1:500, cat# C7113, Sigma) or rabbit anti-P2X3 (1:500, cat# NBP2-33848, Novus Biologicals) respectively (overnight, 4°C). Slides were washed and incubated with donkey anti-mouse Alexa Fluor® 488 or donkey anti-rabbit Alexa Fluor® 555 (1:1000, ThermoFisher) (1 hour, RT). For human tissue, images were captured as stitched Z stacks using Keyence BZ-X800E fluorescence microscope. Cells positive for *Ntrk1*, *Nrp1* and *Gipc1* were counted to mark positive cells, where 10+ fluorescent puncta were considered to be positive.

Human DRG cultures. Human DRG suspension cells were from AnaBios Corporation. Cells were recovered with a gentle centrifugation (RT, 3 min) and resuspension with DMEM/F12 medium containing 10% horse serum, 1% penicillin-streptomycin, 25 ng/ml hNGF and 25 ng/ml GDNF. Cells

were seeded on poly-D-lysine (0.1 mg/ml) and laminin (1 mg/ml)-coated 12-mm glass coverslips. Half of the culture medium was replaced with fresh medium every 3 days. Cultures used within 96 h.

Mouse DRG cultures. C57BL/6 mice (~3-4 weeks) were anaesthetized (5% isoflurane). Thoracic and lumbar DRG were excised and dissociated with collagenase type I (1 mg/ml) and neutral protease (0.62 mg/ml; 45 min, 37°C) under gentle agitation. Dissociated cells were pelleted and resuspended in DMEM containing 10% FBS and 1% penicillin-streptomycin. For siRNA transfection, cells were resuspended in Nucleofector® transfection reagent containing GIPC1 or Ctrl siRNA (500 nM) and a plasmid encoding the enhanced green fluorescent protein (eGFP, 1 µg). Cells were electroporated using Amaxa Biosystem (Lonza) with protocol O-003. Neurons were plated on glass coverslips pretreated with poly-D-lysine (0.1 mg/ml) and laminin (0.01 mg/ml; 30 min). Neurons were used within 48 h and siRNA transfection verified by eGFP fluorescence.

Whole-cell patch-clamp recordings of action potentials and rheobase. DRG neurons were preincubated with EG00229 (30 µM, 30 min) or vehicle (0.1% DMSO) and then challenged with mouse or human NGF (50 nM, 30 min). For current-clamp recordings, the external solution contained (mM): 154 NaCl, 5.6 KCl, 2 $CaCl_2$, 1 $MgCl_2$, 10 D-Glucose, and 8 HEPES (pH 7.4 adjusted with KOH, and mOsm/L= 300). The internal solution comprised (mM): 137 KCl, 10 NaCl, 1 $MgCl_2$, 1 EGTA, and 10 HEPES (pH 7.3 adjusted with KOH, and mOsm/L= 277). Recordings of action potentials were made at RT in whole-cell patch clamp configuration and current-clamp mode. DRG neurons with a resting membrane potential (RMP) more hyperpolarized than −40 mV, stable baseline recordings, and evoked spikes that overshot 0 mV were used for experiments and analysis. Action potentials were evoked by a ramp pulse from 0-1000 pA in 1 sec for human DRG, or 0-250 pA in 1 sec for mouse DRG. Rheobase was measured by injecting currents from 0 pA with an increment of 50 pA in 100 msec (human) or 10 pA in 50 msec (mouse). Results were analyzed using Fitmaster software (HEKA) and Origin 9.0 software (OriginLab).

Whole-cell patch-clamp recordings of Ca^{2+} and Na^{+} currents. DRG neurons were preincubated with EG00229 (30 µM, 30 min) or vehicle (0.1% DMSO) and then challenged with mouse or human NGF (50 nM, 30 min). Ca^{2+} currents (ICa^{2+}) and Na^{+} (INa^{+}) currents were recorded as described (16, 17). In brief, peak Ca^{2+} current was acquired by applying 200 msec voltage steps from −70 to +70 mV in 10 mV increments from a holding potential of −90 mV to obtain the current-voltage (I-V) relation. Peak Na^{+} current was acquired by applying 150 msec voltage steps from −70 to +60 mV in 5 mV increments from a holding potential of −60 mV to obtain the current-voltage (I-V) relation. Capacitive artifacts were fully compensated, and series resistance was compensated by ∼70 %. Recordings made from cells with greater than a 20% shift in series resistance compensation error were excluded from the analysis. All recordings were made at RT (∼23 °C). Results were analyzed with Patchmaster software.

NGF-evoked nociception. Mouse NGF (50 ng/10 µl) was administered by i.pl. injection into the right hindpaw of mice. EG00229, compound 5 (1), a human monoclonal anti-NRP1 antibody (Vesencumab), or IgG control (Ctrl) was administered (i.pl.) concomitantly with NGF. GIPC1 or Ctrl siRNA was administrated (i.t) 48 h before NGF (i.pl.).

Inflammatory pain. CFA (1 mg/ml) or vehicle (0.9% NaCl) was administered (10 µl, i.pl.) into the right hindpaw of sedated mice (2% isoflurane). NRP1 inhibitors were injected (i.pl.) 48 h after CFA. GIPC1 or Ctrl siRNA was administrated (i.t) 24 h after CFA.

Intrathecal administration of siRNA. Mouse GIPC1 or Ctrl siRNA (1.25 µg) was mixed with *in vivo*-jetPEI transfection reagent (8:1 PEI:DNA; Polyplus, 201-50G) and administered to conscious mice (5 µl, i.t., L4-L5), 48 h before NGF (i.pl.) or 24 h after CFA (i.pl.). *Gipc1* mRNA in DRG (L4-L5) was analyzed by RNAScope™ *in situ* hybridization, 48 h after siRNA injection.

Nociception assays. Investigators were blinded to treatments. Mechanical allodynia was assessed by measuring hindpaw withdrawal response to VFF stimulation using the up-and-down method (15). The Hargreaves apparatus was used to evaluate hypersensitivity to heat (Ugo Basile) (15).

Phosphorylated TrkA assays. Acutely dispersed mouse DRG neurons were plated onto coverslips pre-coated with Cell-Tak (30 min, 37°C; CB-40240) in DMEM containing 10% FBS. After 18 h, neurons were incubated with a monoclonal NGF antibody (1:500, 4 h, 37°C; MA5-41968) in serum-free DMEM to reduce interference from endogenous NGF. Neurons were washed in HBSS/0.1% BSA, pre-incubated with EG00229 (30 µM, 30 min) or control, then stimulated with vehicle or murine NGF (100 nM, 15 min, 37°C). Neurons were fixed with 4% paraformaldehyde in PBS (20 min, 4°C), blocked (2% BSA, 0.2% Triton-X-100 in PBS), and incubated with a rabbit mAb to phosphorylated TrkA Y785/TrkB Y816 (1:500, overnight, 4°C; Cell Signaling, 4168). Neurons were washed in PBS and incubated with donkey anti-rabbit Alexa Fluor® 488 (1:1:000, 1 h, RT). Slides were incubated with DAPI, mounted then imaged using a Leica SP8 confocal microscope with HCX PL APO 40x (NA 1.30) oil objective. Mean fluorescence intensity was quantified from regions of interest drawn using a phase contrast image with the maximum projection from four Z planes (0.5 µm thickness). Images were quantified from 34-44 individual cells across three independent experiments using separate mice.

ERK activity FRET biosensor assays. CAD.a cells were serum-starved and transfected with EKAR FRET biosensors (300 ng/well) and human SnapTag-TrkA (150 ng/well). HEK293T-FLPN cells were transfected with FRET biosensors (1 µg/10 cm dish), SnapTag-TrkA (1 µg), and pcDNA3.1 or HaloTag-NRP1 (2 µg). After 24 h, cells were transferred to 96-well plates and serum-starved overnight. On the day of the assay, cells were washed and incubated in Hanks' buffered saline solution (HBSS, pH 7.4) containing 0.1% BSA. After 30 min (37°C), FRET was measured at 60 s intervals (CLARIOstar, BMG Labtech). After 5 baseline reads, cells were stimulated with NGF (0.1 pM-10 nM) or phorbol 12,13-dibutyrate (PDBu, 10 µM). **Δ**FRET represents the ratio (YFP/CFP), minus the mean from 5 initial reads and baseline-corrected to vehicle. Area under the curve (AUC) was determined for each replicate.

ERK transcriptional assays. HEK293T-FLPN cells were transfected with SRE-Luc2P (3 µg/10 cm dish), SnapTag-TrkA (1 µg) and either pcDNA3.1 or HaloTag-NRP1 (2 µg). After 24 h, cells were transferred to 96-well plates. CAD.a cells were transfected with SRE-Luc2P (250 ng/well, 96-well plate), SnapTag-TrkA (150 ng/well) and 100 nM siRNA. After 24 h, cells were serum-starved overnight. Cells were then incubated in HBSS/0.1% BSA and stimulated with NGF (1 pM-10 nM) or PDBu (10 µM). After 5 h stimulation (37ºC), cells were incubated with luciferin (1:2) and lysis buffer (1:5). After 5 min to enable the substrate reaction, luminescence emissions were recorded (CLARIOstar).

Live imaging. HEK293T cells were transfected with SnapTag-TrkA (1 µg/10cm dish), HaloTag-NRP1 (2 µg) or both TrkA and NRP1. After 24 h, cells were transferred to 35 mm dishes. CAD.a cells were seeded in 35 mm dishes, serum-starved for 24 h, and then transfected with SnapTag-TrkA (250 µg/35 mm), HaloTag-NRP1 (500 µg) or both. The next day, proteins were labeled with SNAP-Surface® Alexa Fluor® 488 and membrane-impermeant HaloTag® Alexa Fluor® 660 (0.5 µM, 30 min, 37ºC). Cells were washed in HBSS and imaged on the Leica SP8 confocal.

Receptor-receptor BRET. For endpoint studies, HEK293T cells were transfected with a fixed concentration of NanoLuc-NRP1, NanoLuc-p75^{NTR} or NanoLuc-TrkA (10 ng/well, 96-well plate) and increasing concentrations of SnapTag-TrkA or SnapTag-CALCRL (0-50 ng/well). For kinetic studies, cells were transfected with NanoLuc-TrkA (10 ng/well), SnapTag-TrkA (25 ng/well) and either pcDNA3.1 or HaloTag-NRP1 (50 ng/well). After 48 h, cells were incubated with SNAP-Surface® Alexa Fluor® 488 (0.5 µM, 30 min, 37ºC), washed in HBSS before fluorescence emissions were measured (Synergy Neo2). In some conditions, cells were incubated with NGF (30 nM, 30 min, 37ºC) or vehicle. Cells were then incubated with furimazine (10 µM, 5 min, Promega). For kinetic studies, cells were stimulated with increasing NGF concentrations (1 pM-100 nM) following 5 baseline reads. Luminescence and fluorescence emissions were quantified (Synergy Neo2; BRET1 filter).

Quantifying SNAP-Surface® Alexa Fluor® 488. HEK293T cells were transfected with SnapTag-TrkA (25 ng/well, 96-well plate) and pcDNA3.1 or HaloTag-NRP1 (50 ng/well). CAD.a cells were transfected with SnapTag-TrkA (150 ng/well) and either pcDNA3.1 or HaloTag-NRP1 (300 ng/well). Cells were labeled using SNAP-Surface® Alexa Fluor® 488 and HaloTag® Alexa Fluor® 660 (0.5

µM, 30 min, 37ºC), washed in HBSS/0.1% BSA and fluorescence emissions were recorded (CLARIOstar).

BRET trafficking. HEK293T cells were transfected with TrkA-HA-Rluc8 (15 ng/well, 96-well plate) and a fluorescent marker (15 ng/well) for the plasma membrane (RGFP-CAAX), early endosome (tdRGFP-Rab5a), recycling endosome (tdRGFP-Rab4a) or cis-Golgi apparatus (tdRGFP-Giantin). In some conditions, cells were co-transfected with pcDNA3.1 or HaloTag-NRP1 (30 ng/well), or 100 nM siRNA. Alternatively, CAD.a cells were transfected with TrkA-HA-Rluc8 (125 ng/well) in the absence or presence of HaloTag-NRP1 (250 ng/well), as well as RGFP-CAAX, tdRGFP-Rab5a, tdRGFP-Rab4a or tdRGFP-Giantin (150 ng/well). After 48 h, cells washed in HBSS/0.1% BSA were pre-incubated (30 min, 37ºC) with hypertonic sucrose (0.45 M), Pitstop 2 (30 µM; Abcam), an inhibitor of GIPC1 (CR1023, 300 µM) or its negative control (CR2055), or an inhibitor of myosin VI (TIP, 50 µM). Cells were incubated with coelenterazine purple (25 µg/ml, 10 min, Nanolight). For kinetic studies, 5 baseline reads were measured, then cells were stimulated with NGF (1 pM-100 nM), using 30 nM NGF for endocytic inhibitors. BRET ratios were recorded every 45 s (Synergy Neo2; BRET2 filter: donor 410 ± 80 nm, acceptor 515 ± 30 nm). **Δ**BRET represents BRET in the presence of agonist, minus the vehicle BRET over time. For endpoint studies lacking agonist stimulation, BRET ratios were baseline-corrected to TrkA-HA-Rluc8 expression alone (100%).

Quantitative PCR (qPCR). RNA was isolated from cells or snap-frozen tissues using Direct-zol RNA MiniPrep Kit (Zymo Research, R2050). cDNA was prepared using MultiScribe Reverse Transcriptase (Thermo Fisher, 4311235). cDNA was amplified for 40 cycles by qRT-PCR using the QuantStudio 3 Real-Time PCR System and TaqMan Fast Advanced PCR Mastermix (4444556). Primers to hTrkA (Hs01021011_m1), mTrkA (Mm01219406_m1), hNgfr (Hs00609976_m1), mNgfr (Mm00446296_m1), hGIPC1 (Hs00991802_m1), mGIPC1 (Mm00457561_m1), or GAPDH (Mn99999915_g1) were used. The relative abundance of mRNA was calculated as described (15).

Data analysis. Data presented as mean ± SEM using GraphPad Prism (8.0). Images processed using ImageJ. Illustrations were produced using Adobe Illustrator, Mol*Viewer or BioRender. Concentration-response data fit using non-linear regression analysis as log *vs.* response (three parameters) to determine EC_{50} values. Differences were assessed using paired or unpaired t-test for two comparisons, and 1- or 2-way ANOVA and Tukey's, Dunnett's or Šidák's post-hoc test for multiple comparisons. $P<0.05$ was considered significant at the 95% confidence level.

SI Figures

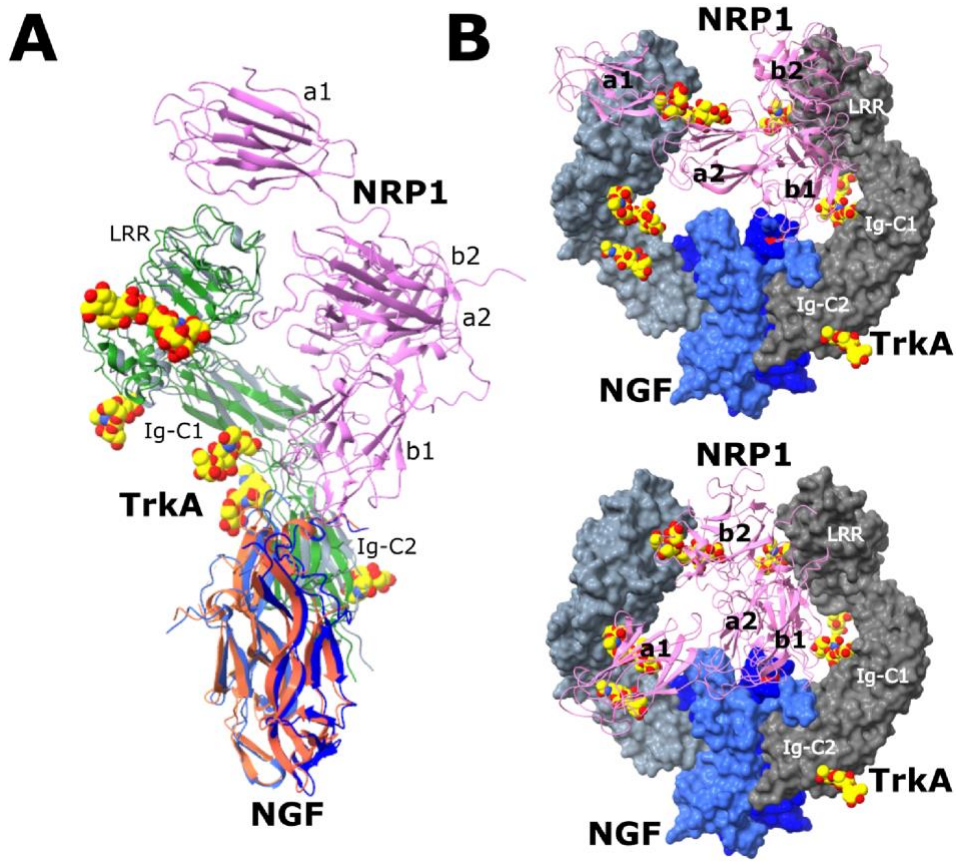

Figure S1. NGF/TrkA/NRP1 docked models in the context of glycosylated TrkA extracellular domains. A. Side view of structural superposition of NGF/TrkA/NRP1 (cartoon, blue/grey/pink) docked model and NGF/TrkA (cartoon, orange/green) crystal structure (PDB 2IFG) through common NGF/TrkA component is shown (only monomers are shown for NRP1 and TrkA for clarity). Asn-linked glycosylations on TrkA in NGF/TrkA crystal structure are shown as space-filling representation and colored according to atom type (C/O/N, yellow/red/blue). Individual domains are labeled and described in text. In cellular context, this comparison shows a glycosylated TrkA compatible binding mode of NRP1 in the docked NGF/TrkA/NRP1 model. **B.** Other docked poses of NRP1 observed in NGF/TrkA/NRP1 docking calculations are shown. Only one monomer of NRP1 (cartoon, pink) bound to NGF/TrkA (surface, blue/grey shades) is shown. For context, TrkA Asn-linked glycosylations are shown in space-filling representations. Individual domains are labeled and described in the text. In contrast to NGF/TrkA/NRP1 docked model described in text, one NRP1 molecule binds to two TrkA monomers at once thereby bridging TrkA dimers in these docked poses. Although NRP1 domains appear to interfere with TrkA glycosylations, domain flexibility in the cellular context (not accounted for in docking calculations) may allow these scenarios to exist. It is important to note that in different docked poses from docking calculations, NRP1 b1 domain still binds to NGF C-terminus in a similar manner while NRP1 a1, a2 and b2 domains are oriented differently.

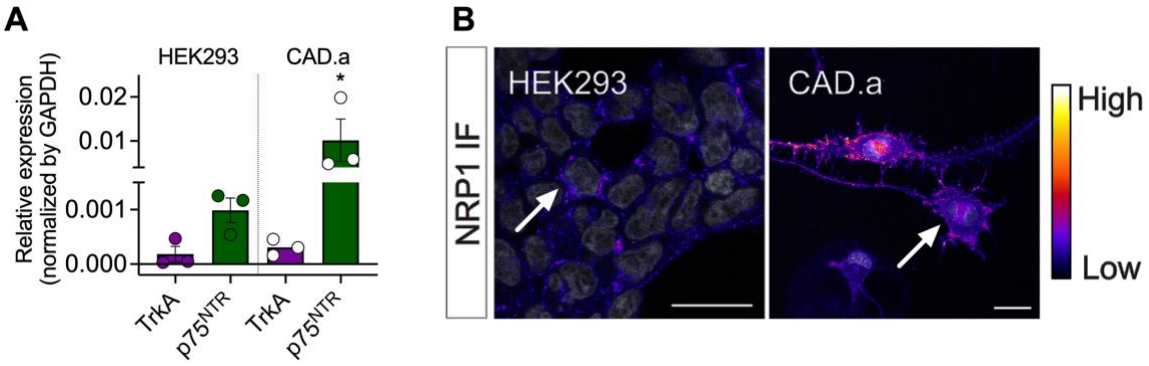

Figure S2. Characterization of receptor expression in neuron-like CAD.a cells. **A.** Quantification of expression of *Ntrk1* mRNA (TrkA) or *Ngfr* ($p75^{NTR}$) in HEK293T or CAD.a cells determined by quantitative RT-PCR. Data from 3 independent experiments with triplicate wells. **B.** Immunofluorescence (IF) staining of NRP1 in HEK293T or CAD.a cells using vesencumab. Scale bar, 20 µm. Representative image from 4 independent experiments. Mean±SEM. *P<0.05. 1-way ANOVA, Dunnett's multiple comparisons.

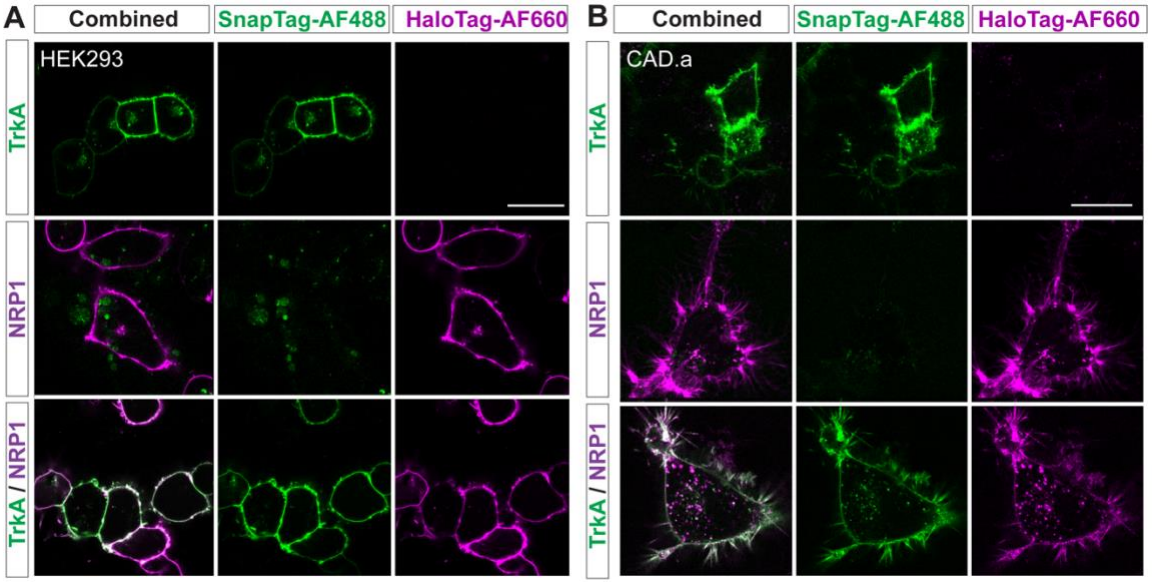

Figure S3. Specificity of SnapTag- and HaloTag- labeling in live cells. HEK293T cells (**A**) or CAD.a cells (**B**) were transfected with SnapTag-TrkA, HaloTag-NRP1 or both (1:2 TrkA to NRP1 ratio). Tags were simultaneously labeled with membrane-impermeant substrate (SNAPTag-Alexa Fluor® 488, HaloTag-Alexa Fluor® 660). Representative from n=5 independent experiments. Scale bar, 20 µm.

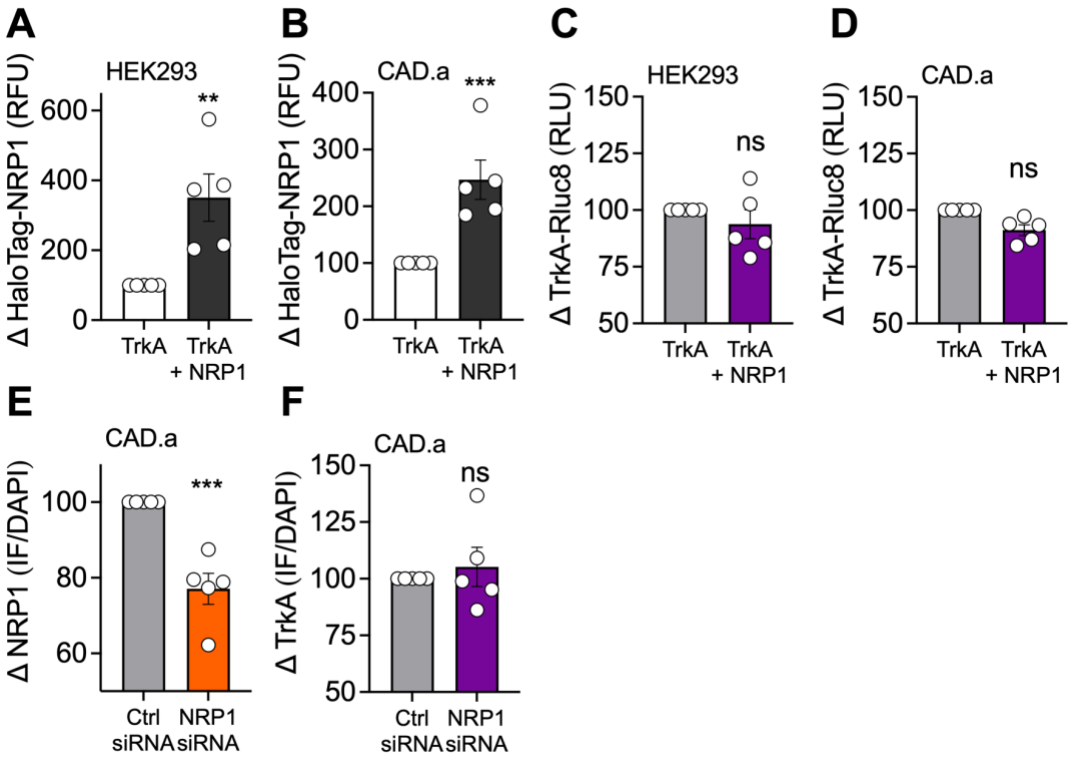

Figure S4. Effect of co-expression or siRNA on TrkA and NRP1 expression. **A-D.** NRP1 and TrkA expression in HEK293T (**A, C**) or CAD.a (**B, D**) cells expressing TrkA-Rluc8 in the absence or presence of HaloTag-NRP1. **A, B.** Cells were labeled with membrane-impermeant HaloTag-Alexa Fluor® 660 and emissions were measured as relative fluorescence units (RFU). **C, D.** TrkA-Rluc8 emissions were measured after incubation with coelenterazine purple to infer TrkA expression as relative luminescence units (RLU). **E, F.** Effect of NRP1 siRNA on expression of NRP1 (**E**) or TrkA (**F**) quantified using immunofluorescence staining normalized to nuclei count (DAPI). Data expressed as percentage change over control (100%). Data from 5 independent experiments. Mean±SEM. ***P*<0.01, *** *P*<0.001, ns, not significant. Unpaired t-test.

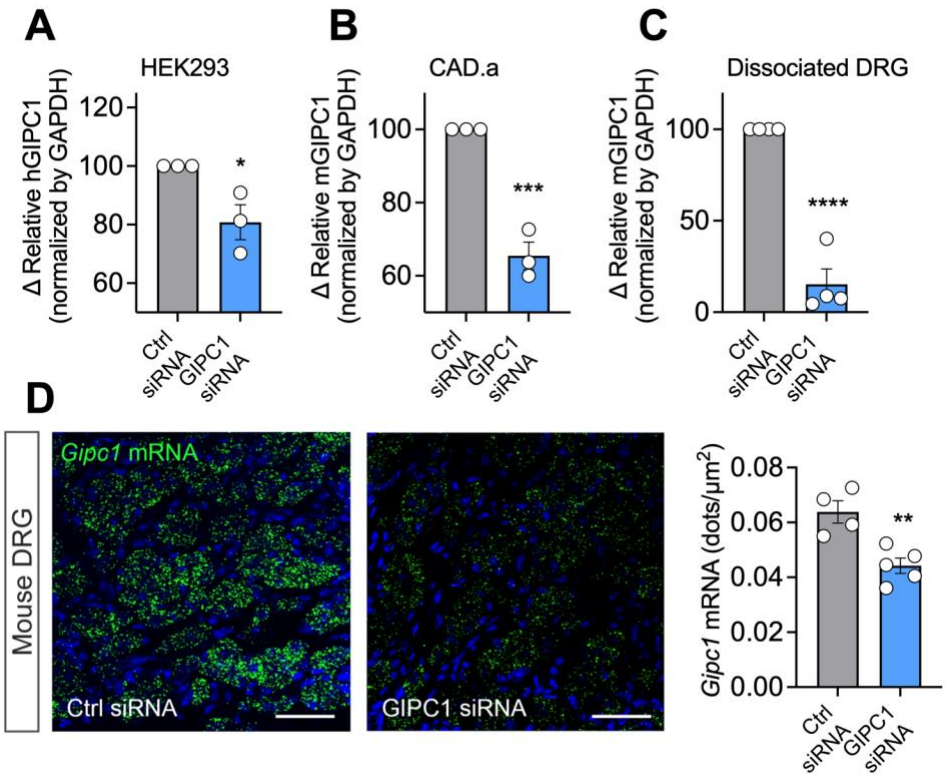

Figure S5. Confirmation of GIPC1 knockdown using siRNA. A-C. Quantification of expression of *Gipc1* mRNA in HEK293T (**A**), CAD.a cells (**B**) or cultured dissociated DRG neurons (**C**) in the presence of control (Ctrl) or GIPC1 siRNA determined by quantitative RT-PCR. Data from 3-4 independent experiments with triplicate wells. **D.** RNAScope™ localization of *Gipc1* mRNA in murine DRG after intrathecal injection of Ctrl or GIPC1 siRNA. Representative image from n=5 mice. Mean±SEM. *P<0.05, **P<0.01, *** P<0.001, **** P<0.0001. Unpaired t-test.

SI Tables

Table S1. Interfacing residues between NRP1-NGF and NRP1-TrkA in NRP1/NGF/TrkA ternary computational model.

NRP1 (monomer 1)		NGF (monomer 1)	
Residue	**H (Hydrogen bond) S (Salt Bridge)**	**Residue**	**H (Hydrogen bond) S (Salt Bridge)**
Tyr297		His75	
Trp301		Trp76	
Thr316		Arg114	H
Pro317		Ala116	
Gly318		Val117	
Glu319		Arg118	HS
Asp320	HS		
Lys351			
Tyr353	H		
Thr413	H		
Gly414			
NRP1 (monomer 1)		**NGF (monomer 2)**	
Residue	**H (Hydrogen bond) S (Salt Bridge)**	**Residue**	**H (Hydrogen bond) S (Salt Bridge)**
Asp320		Ser2	H
Thr349		Ser3	
Lys351		Phe7	
Tyr354		His8	
Lys356	H	Ser73	
Thr357			
Thr410			
Trp411			
Glu412			
Thr413			
NRP1 (monomer 1)		**TrkA (monomer 1)**	
Residue	**H (Hydrogen bond) S (Salt Bridge)**	**Residue**	**H (Hydrogen bond) S (Salt Bridge)**
Ile107		Cys36	
Ala108		Pro37	
Pro110		Asp38	
Pro201		Ser46	
Gly202	H	Arg52	
Gly203		Ala65	
Met204		Glu66	
Lys373	S	Asn67	H
Asn376	H	Leu68	
Lys377	S	Thr69	
Pro378		Glu92	
		Arg94	
		Glu231	S
		Glu233	HS
		Gln234	H
		Asp257	S

Interface calculations are made using PISA (13). C-terminal Arg118 from NGF and residues of C-terminal arginine binding pocket from b1 domain of NRP1 are in red. Residues predicted to form or possibly form hydrogen bonds (H) or salt bridges (S) are also indicated

Table S2. Gating properties of Ca^{2+} and Na^{+} currents recorded from mouse DRG neurons.

Total Ca^{2+}	**DMSO (0.1%)**	**EG00229 (30 µM)**	**NGF (50 nM)**	**EG00229 + NGF**
Activation				
$V_{1/2}$	5.793 ± 1.891 (10)	-2.828 ± 0.871 (6)†	5.834 ± 1.995 (9)††	-0.473 ± 1.265 (8)
k	7.756 ± 1.534 (10)	4.230 ± 0.731 (6)	7.972 ± 1.608 (9)	6.428 ± 1.109 (8)
Inactivation				
$V_{1/2}$	-27.372 ± 1.919 (9)	-20.137 ± 0.901 (7)	-23.909 ± 3.080 (9)	-20.166 ± 1.314 (8)
k	-14.944 ± 2.109 (9)	-10.623 ± 0.842 (7)	-15.079 ± 3.305 (9)	-13.176 ± 1.287 (8)
Total Na^{+}	**DMSO (0.1%)**	**EG00229 (30 µM)**	**NGF (50 nM)**	**EG00229 + NGF**
Activation				
$V_{1/2}$	-22.436 ± 1.150 (10)	-23.229 ± 0.499 (13)	-23.151 ± 0.418 (14)	-23.600 ± 0.993 (11)
k	5.098 ± 1.014 (10)	3.580 ± 0.434 (13)	3.432 ± 0.362 (14)	5.145 ± 0.877 (11)
Inactivation				
$V_{1/2}$	-48.736 ± 4.219 (10)	-43.306 ± 4.249 (13)	-54.450 ± 2.244 (14)	-38.622 ± 4.013 (11)*
k	-18.568 ± 4.934 (10)	-21.036 ± 5.439 (13)	-14.748 ± 2.243 (14)	-19.732 ± 4.708 (11)

Values are mean±SEM calculated from fits of the data from the indicated number of individual cells (in parentheses) to the Boltzmann equation; $V_{1/2}$ midpoint potential (mV) for voltage-dependent of activation or inactivation; *k*, slope factor. Data were analyzed with 1-way ANOVA with Tukey's multiple comparisons. † p=0.0115 for $V_{1/2}$ activation of EG00229 vs DMSO (0.1%); †† p=0.0131 for $V_{1/2}$ activation of NGF vs EG00229; * p= 0.0175 for $V_{1/2}$ inactivation of EG00229 + NGF vs DMSO (0.1%).

Table S3. Pharmacological parameters (pEC_{50}) of NGF derived in at human TrkA, in the absence or presence of NRP1 modulation.

CAD.a cells	**Control**	**NRP1 inhibition (EG00229)**
Cytosolic ERK (FRET)	10.64 ± 0.41 (5)	10.53 ± 0.17 (5)
Nuclear ERK (FRET)	11.09 ± 0.33 (5)	10.01 ± 0.38 (5) *
HEK293T cells	**Control**	**NRP1 overexpression (HaloTag)**
Cytosolic ERK (FRET)	9.89 ± 0.21 (5)	9.87 ± 0.10 (4)
Nuclear ERK (FRET)	10.37 ± 0.19 (5)	10.59 ± 0.33 (5)
ERK Transcription (SRE-Luc2P)	9.67 ± 0.48 (8)	10.15 ± 0.57 (8) ***
TrkA-Rluc8 Trafficking (BRET)	9.06 ± 0.10 (6)	9.08 ± 0.13 (6)
TrkA/TrkA Oligomerization (BRET)	7.81 ± 0.07 (4)	7.87 ± 0.04 (5)

Derived in HEK293T or neuron-like CAD.a cells transfected with full-length, human TrkA. Values are mean±SEM calculated from non-linear regressions fit of the data from independent replicates (in parentheses), each with triplicate wells. Quantified as the negative antilog of the half-maximal effective concentration ($pEC_{50} = -\log EC_{50}$). *P<0.05, ***P<0.001. Paired t-test.

Table S4. siRNA sequences used in this study.

Target	Sequence
Control	UGGUUUACAUGUCGACUAA UGGUUUACAUGUUGUGUGA UGGUUUACAUGUUUUCUGA UGGUUUACAUGUUUUCCUA
mNrp1	GAAUUGCUGUGGAUGAUAU AGUAAGAGGUGUCAUCAUU CCACAAGGUUCAUCAGGAU GGAAUGUUCUGUCGCUAUG
hGipc1	GCACUCGGGCUCACCAUCA GGCCGUACCUUCACGCUGA GCAAGGCCUUCGACAUGAU CUGGAGAGUUACAUGGGUA
mGipc1	GCAUCGAGGGCUUCACUAA CGUCGGCCUUUGAGGAGAA GUGGAUGACUUGCUAGAGA GCUGAGGCCUUCCGACUAC

SI References

1. S. Perez-Miller *et al.*, Novel Compounds Targeting Neuropilin Receptor 1 with Potential To Interfere with SARS-CoV-2 Virus Entry. *ACS Chem Neurosci* **12**, 1299-1312 (2021).
2. A. S. Dixon *et al.*, NanoLuc Complementation Reporter Optimized for Accurate Measurement of Protein Interactions in Cells. *ACS Chem Biol* **11**, 400-408 (2016).
3. J. Jumper *et al.*, Highly accurate protein structure prediction with AlphaFold. *Nature* **596**, 583-589 (2021).
4. M. W. Parker, P. Xu, X. Li, C. W. Vander Kooi, Structural Basis for Selective Vascular Endothelial Growth Factor-A (VEGF-A) Binding to Neuropilin-1*. *Journal of Biological Chemistry* **287**, 11082-11089 (2012).
5. T. Teesalu, K. N. Sugahara, V. R. Kotamraju, E. Ruoslahti, C-end rule peptides mediate neuropilin-1-dependent cell, vascular, and tissue penetration. *Proc Natl Acad Sci U S A* **106**, 16157-16162 (2009).
6. A. Fiser, R. K. G. Do, A. Šali, Modeling of loops in protein structures. *Protein Science* **9**, 1753-1773 (2000).
7. G. C. P. van Zundert *et al.*, The HADDOCK2.2 Web Server: User-Friendly Integrative Modeling of Biomolecular Complexes. *Journal of Molecular Biology* **428**, 720-725 (2016).
8. A. Saponaro, V. Maione, A. Bonvin, F. Cantini, Understanding Docking Complexes of Macromolecules Using HADDOCK: The Synergy between Experimental Data and Computations. *BIO-PROTOCOL* **10** (2020).
9. B. J. C. Janssen *et al.*, Neuropilins lock secreted semaphorins onto plexins in a ternary signaling complex. *Nature Structural & Molecular Biology* **19**, 1293-1299 (2012).
10. C. W. Vander Kooi *et al.*, Structural basis for ligand and heparin binding to neuropilin B domains. *Proc Natl Acad Sci U S A* **104**, 6152-6157 (2007).
11. Anonymous.
12. E. Krissinel, K. Henrick, Inference of Macromolecular Assemblies from Crystalline State. *Journal of Molecular Biology* **372**, 774-797 (2007).
13. W. L. DeLano, The PyMOL molecular graphics system. *http://www. pymol. org/* (2002).
14. E. C. Meng *et al.*, UCSF ChimeraX: Tools for structure building and analysis. *Protein Science* **32**, e4792 (2023).
15. R. Tonello *et al.*, The contribution of endocytosis to sensitization of nociceptors and synaptic transmission in nociceptive circuits. *Pain* **164**, 1355-1374 (2023).
16. A. Moutal *et al.*, SARS-CoV-2 spike protein co-opts VEGF-A/neuropilin-1 receptor signaling to induce analgesia. *Pain* **162**, 243-252 (2021).
17. K. Gomez *et al.*, Neuropilin-1 is essential for vascular endothelial growth factor A-mediated increase of sensory neuron activity and development of pain-like behaviors. *Pain* 10.1097/j.pain.0000000000002970 (2023).